Construction of Distinct Discrete Time Scattering Quantum Walk Formulations on the Honeycomb Lattice

Marcos G. E. da Luz[§]

XXI International Conference:
Geometry, Integrability and Quantization

Jun 03-08 (2019), Varna, Bulgaria

[§]Universidade Federal do Paraná-UFPR
Curitiba-PR, Brazil

Collaborators:

Bruno. F. Venancio
Military College-PR
Opet College

Annals of Physics **396**, 517-545 (2018)

Outline

- Why Quantum Walks (QW) are interesting
- A gentle introduction: QW in 1D
- Quantizing QW for the honeycomb lattice (very relevant in quantum matter physics, due its particular topology, for instance, graphene)
- Topology is essential
- Proper time evolution + particular topology + symmetries of the lattice → lead to a finite number of possible quantizations (i.e, acceptable time evolution operators)
- Explicit analytical functions are necessary to "characterize" the graph (lattice) topology: one should concretely construct the time evolution operator U.

QW overview [Geometry (Topology) and Quantization]

- Quantum walks (introduced in the 1990's, but Dirac equation: Feynman): elementary models of quantum mechanics (QM), still displaying all their essentials
- Essential in quantum computation: algorithms (as oracular [black box], element distinctness [differences], triangle finding [a triangle-free graph] problems, NAND [not-and gate] trees and Grover search)
- Nowadays relatively easy to realize: atoms in optical lattices, photons interf., NMR processors, etc
- Allow analytical treatment, many beautiful results proved (e.g., coin and scattering are unitary equivalent)
- More recently: quantum chaos, condensed matter physics and topological effects: QPT, graphene, etc

A brief overview on the 1D case

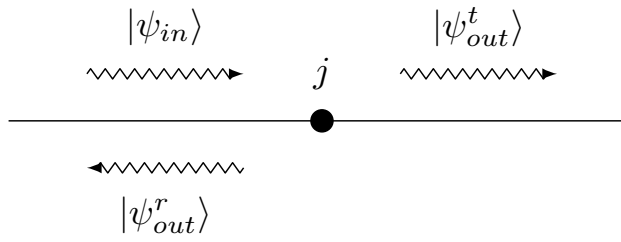

Figure 1: The process of an incoming state $|\psi_{in}\rangle$ scattered off by a point interaction at j, and then being splitted into reflected $|\psi^r_{out}\rangle$ and transmitted $|\psi^t_{out}\rangle$ outgoing states.

$$|\psi_{in}\rangle \to |\psi_{out}\rangle = \Gamma_r|\psi^r_{out}\rangle + \Gamma_t|\psi^t_{out}\rangle, \tag{1}$$

Basis states $\{|\sigma, j\rangle\}$ ($j \in \mathbb{Z}$, $\sigma = \pm 1$). An arbitrary state $|\psi\rangle$ can be generally expressed as $|\psi\rangle = \sum_{\sigma,j} c_{\sigma,j}\,|\sigma, j\rangle$.

$$\begin{aligned} &|\psi_n\rangle = \hat{U}|\psi_{n-1}\rangle, \\ &\hat{U}|\sigma, j\rangle = \Gamma^{(j)}_{-\sigma\,\sigma}\,|-\sigma, j-\sigma\rangle + \Gamma^{(j)}_{\sigma\,\sigma}\,|\sigma, j+\sigma\rangle. \end{aligned} \tag{2}$$

The scattering matrix at each site j,

$$\Gamma^{(j)} = \begin{matrix} \\ {\scriptstyle (-)} \\ {\scriptstyle (+)} \end{matrix} \begin{matrix} \begin{matrix} {\scriptstyle (+)} & \quad {\scriptstyle (-)} \end{matrix} \\ \begin{pmatrix} \Gamma^{(j)}_{-+} & \Gamma^{(j)}_{--} \\ \Gamma^{(j)}_{++} & \Gamma^{(j)}_{+-} \end{pmatrix} \end{matrix}, \tag{3}$$

is such that $\Gamma^{(j)\dagger}\Gamma^{(j)} = \Gamma^{(j)}\Gamma^{(j)\dagger} = \mathcal{I}$ (with $\mathcal{I}$ the identity operator), guaranteeing probability flux conservation.

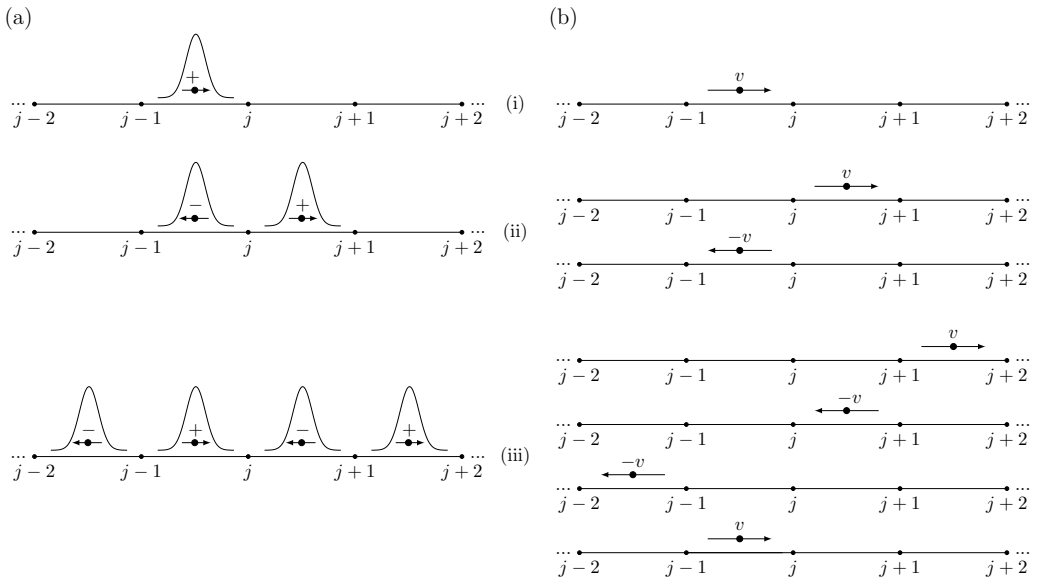

Figure 2: The schematics of the initial configuration (i), and first (ii) and second (iii) time steps — respectively, $n = 0$, and $n = 1$ and $n = 2$ — for the (a) SQW and (b) RW. (a) In the quantum case it is pictorically represented the basis states composing $|\psi_n\rangle$ ($n = 0, 1, 2$). (b) In the classical case it is displayed the possible two (ii) and (iii) four paths to follow at $n = 1$ and $n = 2$.

The probability to visit the site j after step n

$$P_n(j)|_{SQW} = \sum_{\sigma} |\langle \sigma, j|\hat{U}^n|\psi_0\rangle|^2. \tag{4}$$

Example, let us assume that the SQW initial state is

$$|\psi_0\rangle = \frac{1}{\sqrt{2}}\Big(|+1, 0\rangle + i\,|-1, 0\rangle\Big), \tag{5}$$

and that $\forall j$ we have the same unbiased (i.e., equal probabilities of reflections and transmissions) Hadamard scattering matrix

$$\Gamma^{(j)} = \frac{1}{\sqrt{2}} \begin{pmatrix} +1 & +1 \\ +1 & -1 \end{pmatrix}. \tag{6}$$

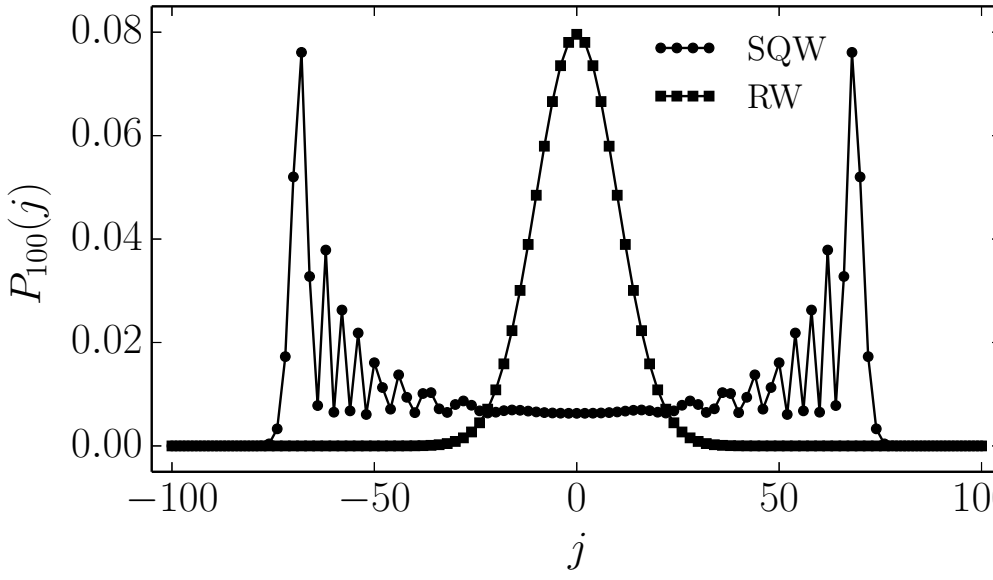

Figure 3: The probability distributions $P_{100}(j)$ for the RW and SQW after 100 time steps. In both cases the probabilities are non-null only for even $|j| \leq 100$ (just the j's shown).

For our classical RW, initially leaving from $x_0 = 0$ to the right and with the symmetric value $p = 1/2$, the probability to be in $x = j\,\ell$ at $t = n\,\tau$ is given by ($j \leq n$ and $n \pm j$ even)

$$P_n(j)|_{RW} = \frac{n!}{\left(\frac{n+j}{2}\right)!\left(\frac{n-j}{2}\right)!}\left(\frac{1}{2}\right)^n. \tag{7}$$

For $n = 100$, the two functions $P_{n=100}(j)$ are shown in Fig. 3. Note that while for the classical RW the distribution is basically a Gaussian centered at the origin (the initial position), for the SQW it is a bimodal distribution presenting higher probabilities for larger $|j|$'s (thus, illustrating the superdiffusive features of QWs).

Time evolution operator for a SQ
on the honeycomb lattice

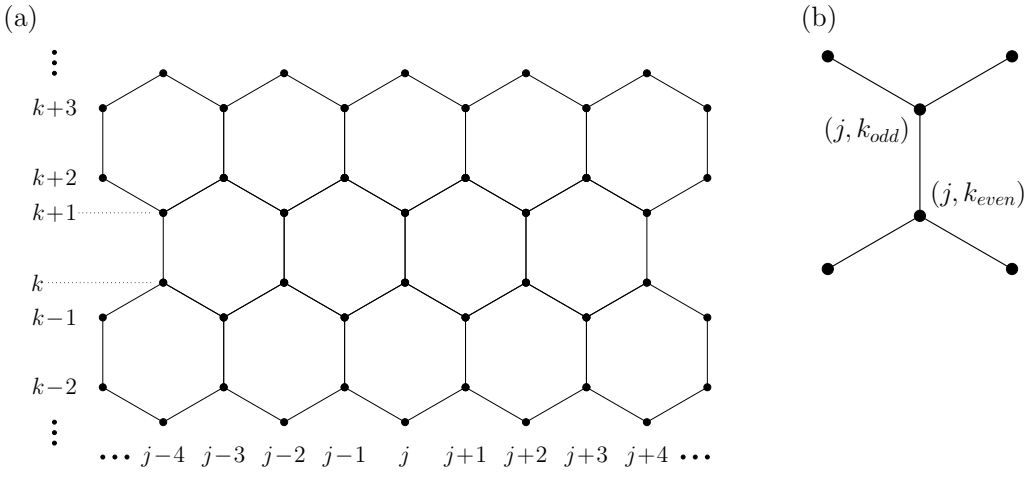

Figure 4: (a) The honeycomb lattice and (b) the convention for the k labeling.

Considering that all bonds (edges) have the same length $\ell = 1$, the cartesian coordinates of the site $v = (j, k)$ are given by

$$x_v(j) = \frac{\sqrt{3}j}{2}, \qquad y_v(k) = \frac{3}{4}\left(k + \frac{1-(-1)^k}{6}\right). \tag{8}$$

The functions $f_m(j,k)$ and $g_m(k)$ give the indices of the three adjacent sites (j_m, k_m) to (j,k). They read $(m = 1, 2, 3)$

$$f_m(j,k) = j + (m-2)(-1)^k \tag{9}$$

and

$$g_m(k) = k + (-1)^{m+k}. \tag{10}$$

$$f_m(f_m(j,k), g_m(k)) = j, \;\; g_m(f_m(j,k), g_m(k)) = k. \tag{11}$$

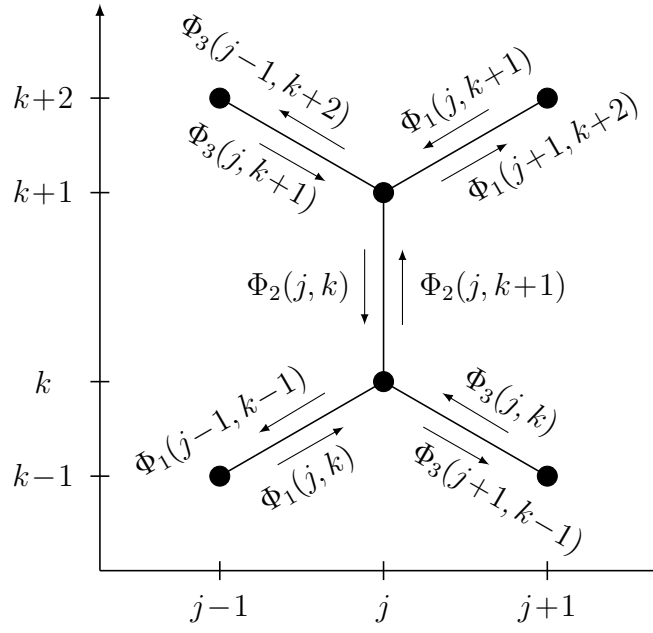

Figure 5: Schematic representation of how the *topological directional function* $\Phi_m(j,k)$ is associated to directions along the lattice bonds.

The quantum Hilbert space is spanned by the orthonormal basis $\{|\sigma,j,k\rangle\}$, representing localized states for a particle evolving towards the site (j,k) along the direction specifyied by the quantum number σ (with $\sigma=\alpha\neq\beta\neq\gamma$).

For $m\in\{1,2,3\}$ an orientationl auxiliary index, we define the *topological directional function* $\Phi_m(j,k)$, as conventioned in Fig. 5, such that $\sigma=\Phi_m(j,k)$.

For uniqueness and consistence of labeling, it follows that

$$\begin{aligned}&\Phi_{m''}(j,k)\neq\Phi_{m'}(j,k)\quad\text{when}\quad m''\neq m'.\\&\Phi_{m''}(f_{m''}(j,k),g_{m''}(k))\neq\Phi_{m''}(f_{m''}(j,k),g_{m''}(k))\quad\text{if}\quad m''\neq m'.\end{aligned}\tag{12}$$

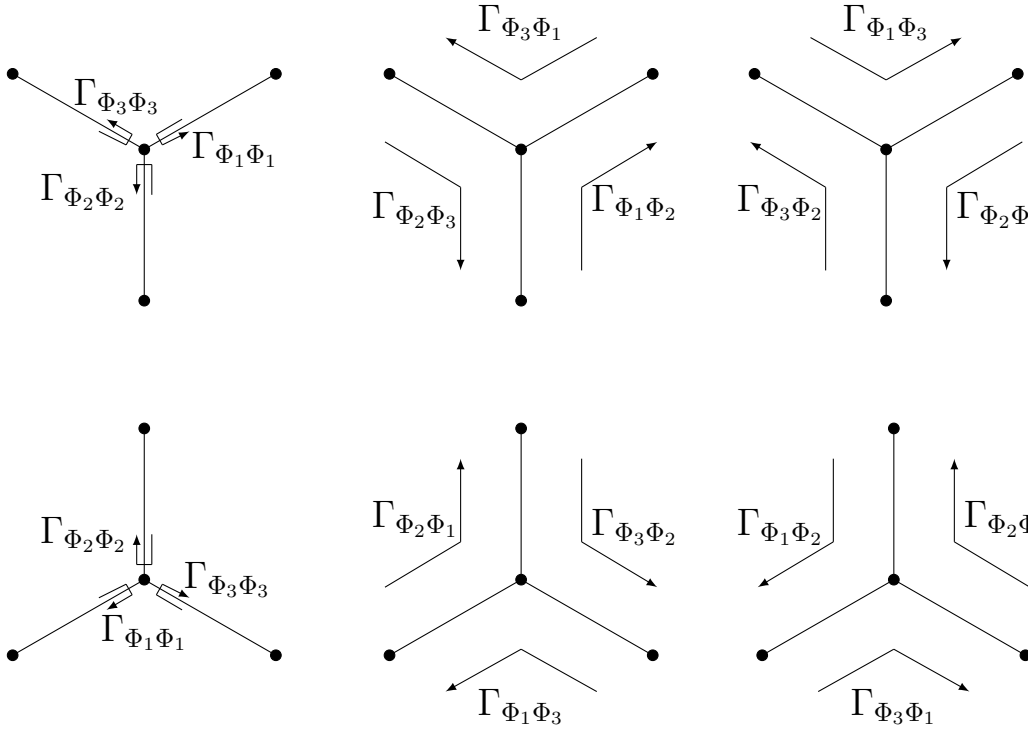

Figure 6: Schematics illustrating to which scattering processes – either reflections (left panels) or transmissions (central and right panels) – by the middle site $v = (j,k)$ the coefficients $\Gamma^{(j,k)}_{\sigma''\sigma'}$ are associated to.

The time evolution is given by ($n \in \mathbb{N}$)

$$|\psi_n\rangle = \hat{U}^n|\psi_0\rangle, \tag{13}$$

The operator $\hat{U}$ is characterized, in each site, by nine coefficients $\Gamma^{(j,k)}_{\sigma''\sigma'}$. They represent the quantum amplitudes for all the scattering processes at any site $v = (j,k)$, as depicted in Fig. 6.

$$\begin{aligned}\hat{U}|\Phi_m(j,k),j,k\rangle &= \sum_{l=1}^{3} \Gamma^{(j,k)}_{\Phi_l(f_l(j,k),g_l(k))\,\Phi_m(j,k)} \\ &\times|\Phi_l(f_l(j,k),g_l(k)),f_l(j,k),g_l(k)\rangle \end{aligned}\tag{14}$$

and

$$\hat{U}^{\dagger}|\Phi_m(j,k),j,k\rangle = \sum_{l=1}^{3} \Gamma^{(f_m(j,k),g_m(k))^*}_{\Phi_m(j,k)\,\Phi_l(f_m(j,k),g_m(k))} \times|\Phi_l(f_m(j,k),g_m(k)),f_m(j,k),g_m(k)\rangle. \tag{15}$$

Since $\hat{U}$ is unitary, it reads

$$\sum_{l=1}^{3} \Gamma^{(j,k)}_{\Phi_l(f_l(j,k),g_l(k))\,\Phi_{m''}(j,k)}\, \Gamma^{(j,k)^*}_{\Phi_l(f_l(j,k),g_l(k))\,\Phi_{m'}(j,k)} = \delta_{m''m'}, \tag{16}$$

$$\sum_{l=1}^{3} \Gamma^{(j,k)^*}_{\Phi_{m''}(f_{m''}(j,k),g_{m''}(k))\,\Phi_l(j,k)}\, \Gamma^{(j,k)}_{\Phi_{m'}(f_{m'}(j,k),g_{m'}(k))\,\Phi_l(j,k)} = \delta_{m''m'}. \tag{17}$$

Eqs. (16) and (17) means $\Gamma^{(j,k)^\dagger}\,\Gamma^{(j,k)} = \Gamma^{(j,k)}\,\Gamma^{(j,k)^\dagger} = \mathcal{I}$.

The scattering amplitudes at each vertex (j,k) (c.f., Fig. 6)

$$\Gamma^{(j,k)} = \begin{pmatrix} \Gamma^{(j,k)}_{\alpha\alpha} & \Gamma^{(j,k)}_{\alpha\beta} & \Gamma^{(j,k)}_{\alpha\gamma} \\ \Gamma^{(j,k)}_{\beta\alpha} & \Gamma^{(j,k)}_{\beta\beta} & \Gamma^{(j,k)}_{\beta\gamma} \\ \Gamma^{(j,k)}_{\gamma\alpha} & \Gamma^{(j,k)}_{\gamma\beta} & \Gamma^{(j,k)}_{\gamma\gamma} \end{pmatrix}, \tag{18}$$

The scattering amplitude $\Gamma^{(j,k)}_{\Phi_m(f_m(j,k),g_m(k))\,\Phi_l(j,k)}$ represents reflection (transmission) if $m = l$ ($m \neq l$), Fig. 6. So

$$\Gamma^{(j,k)}_{\Phi_m(f_m(j,k),g_m(k))\,\Phi_m(j,k)} = r^{(j,k)}_{\Phi_m(f_m(j,k),g_m(k)),\Phi_m(j,k)} \tag{19}$$

and

$$\Gamma^{(j,k)}_{\Phi_m(f_m(j,k),g_m(k))\,\Phi_l(j,k)} = t^{(j,k)}_{\Phi_m(f_m(j,k),g_m(k)),\Phi_l(j,k)}. \tag{20}$$

Calculating the probabilities

Suppose a quantum state in time $n-1$ given by

$$|\psi_{n-1}\rangle = \sum_{m=1}^{3} \sum_{j,k} \psi_{n-1}(m,j,k)\, |\Phi_m(j,k),j,k\rangle. \tag{21}$$

Then, if $\hat{U}|\psi_{n-1}\rangle = |\psi_n\rangle = \sum_{m=1}^{3} \sum_{j,k} \psi_n(m,j,k)\, |\Phi_m(j,k),j,k\rangle$, we get after some algebra that

$$\psi_n(m,j,k) = \sum_{l=1}^{3} \psi_{n-1}(l, f_m(j,k), g_m(k))\, \Gamma^{(f_m(j,k),g_m(k))}_{\Phi_m(j,k)\,\Phi_l(f_m(j,k),g_m(k))}. \tag{22}$$

Thus, the probability to find the particle propagating to (j,k) at time n in terms of the quantum amplitudes in time $n-1$ reads

$$\begin{aligned} P_n(j,k)|_{SQW} &= \sum_{m=1}^{3} |\psi_n(m,j,k)|^2 \\ &= \sum_{m=1}^{3} \left(\sum_{l=1}^{3} \rho^{(j,k)}_{m\,l} |\psi_{n-1}(l, f_m(j,k), g_m(k))|^2 \right) \\ &\quad + \sum_{m,l'',l'=1\,(l''\neq l')}^{3} \Lambda^{(j,k)}_{m\,l''}\, \Lambda^{(j,k)^*}_{m l'}, \end{aligned} \tag{23}$$

where

$$\rho^{(j,k)}_{m\,l} = \left| \Gamma^{(f_m(j,k),g_m(k))}_{\Phi_m(j,k)\,\Phi_l(f_m(j,k),g_m(k))} \right|^2, \tag{24}$$

and

$$\Lambda^{(j,k)}_{m\,l} = \psi_{n-1}(l, f_m(j,k), g_m(j,k))\, \Gamma^{(f_m(j,k),g_m(k))}_{\Phi_m(j,k)\,\Phi_l(f_m(j,k),g_m(k))}. \tag{25}$$

The construction of the topological directional function $\Phi_m(j,k)$

As explained in details in [Phys. Rev. A **80**, 052301 (2009)], the formulation of self-consistent QW models in arbitrary structures requires: (a) a definition of the time evolution operator in terms of functions properly describing the lattice topological features; and (ii) these functions must display few basic (but general) properties. For the present regular network, the topological directional function $\Phi_m(j,k)$ — given the quantum number σ — plays exactly such role. Indeed, the necessary conditions are completely fulfilled by the Eqs. (12), below. Moreover, $\Phi_m(j,k)$ are such that the Bloch's theorem is also observed.

$$\Phi_{m''}(j,k) \neq \Phi_{m'}(j,k) \quad \text{when} \quad m'' \neq m'.$$
$$\Phi_{m''}(f_{m''}(j,k), g_{m''}(k)) \neq \Phi_{m''}(f_{m''}(j,k), g_{m''}(k)) \quad \text{if} \quad m'' \neq m'. \tag{26}$$

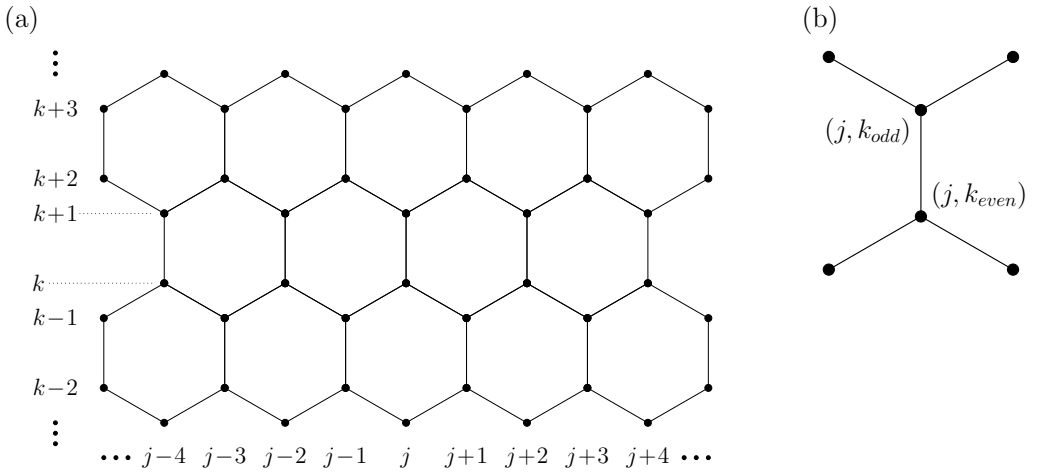

Figure 7: (a) The honeycomb lattice and (b) the convention for the k labeling.

For the construction of $\Phi_m(j,k)$, we recall the convention in Fig. 7 (b). So, based on the lattice symmetry and the geometric distinction associated to the indices j and k, let us write

$$\Phi_m(j,k) = \varphi_m(j)[k+1]_2 + \phi_m(j)[k]_2. \tag{27}$$

Here we define $[x]_y \equiv x \bmod y$, i.e., $[x]_y$ is the remainder of x/y. Hence, if k is even (odd) $[k+1]_2 = 1$ ($[k+1]_2 = 0$) and $[k]_2 = 0$ ($[k]_2 = 1$). The auxiliary φ_m and ϕ_m — functions only of j — can assume just three possible values (because for the honeycomb the coordination number is three). Hence, for $\alpha \neq \beta \neq \gamma$ and $\lambda \neq \kappa \neq \mu$,

$$\varphi \in \{\alpha,\, \beta,\, \gamma\}, \qquad \phi \in \{\lambda,\, \kappa,\, \mu\}. \tag{28}$$

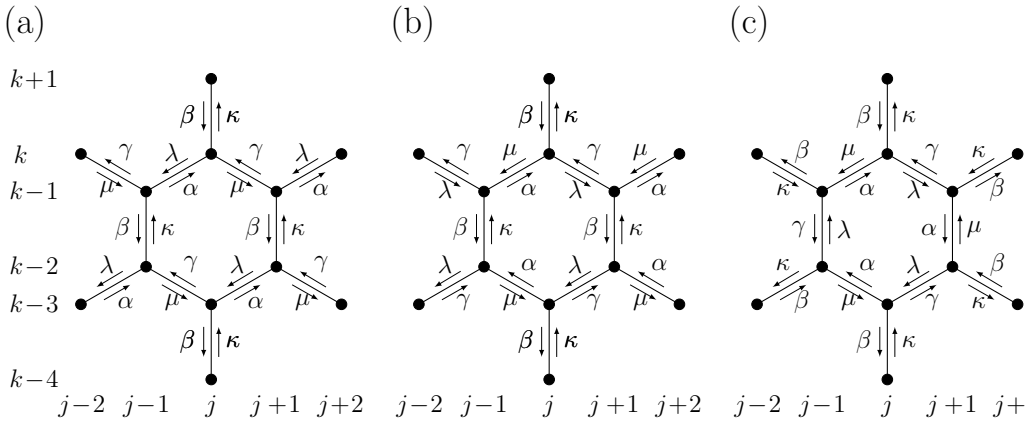

Figure 8: For the *basic segment* of the honeycomb lattice, it is illustrated the three possible ways to ascribe values for the topological directional function $\Phi_m(j,k)$, labeled as: (a) distribution (i), (b) distribution (ii), (c) distribution (iii).

The key point now is how to attribute the values in Eq. (28) to $\varphi_m(j)$ and $\phi_m(j)$ in a way to both, comply with Eqs. (12) and (12), and be compatible with the translational invariance of the honeycomb lattice. A direct analysis shows that there are only three ways to do so, leading to three distinct distributions (i), (ii), and (iii) of values for $\Phi_m(j,k)$ of Eq. (27).

By denoting the structure in Fig. 8 as the *basic segment* of the honeycomb, the possibilities (i), (ii), and (iii) are depicted, respectively, in Fig. 8 (a), (b), and (c).

The possibilities (i), (ii), (iii) (see Fig. 8) are

$$\Phi_1^{(i)}(j,k) = \alpha[k+1]_2 + \lambda[k]_2, \tag{29}$$
$$\Phi_2^{(i)}(j,k) = \beta[k+1]_2 + \kappa[k]_2, \tag{30}$$
$$\Phi_3^{(i)}(j,k) = \gamma[k+1]_2 + \mu[k]_2, \tag{31}$$

$$\Phi_1^{(ii)}(j,k) = \begin{cases} \alpha[k+1]_2 + \lambda[k]_2, & \text{if } [j]_2 = 0, \\ \gamma[k+1]_2 + \mu[k]_2, & \text{if } [j]_2 = 1, \end{cases} \tag{32}$$
$$\Phi_2^{(ii)}(j,k) = \beta[k+1]_2 + \kappa[k]_2, \tag{33}$$
$$\Phi_3^{(ii)}(j,k) = \begin{cases} \gamma[k+1]_2 + \mu[k]_2, & \text{if } [j]_2 = 0, \\ \alpha[k+1]_2 + \lambda[k]_2, & \text{if } [j]_2 = 1, \end{cases} \tag{34}$$

$$\Phi_1^{(iii)}(j,k) = \begin{cases} \alpha[k+1]_2 + \lambda[k]_2, & \text{if } [j]_3 = 0, \\ \gamma[k+1]_2 + \kappa[k]_2, & \text{if } [j]_3 = 1, \\ \beta[k+1]_2 + \mu[k]_2, & \text{if } [j]_3 = 2, \end{cases} \tag{35}$$
$$\Phi_2^{(iii)}(j,k) = \begin{cases} \beta[k+1]_2 + \kappa[k]_2, & \text{if } [j]_3 = 0, \\ \alpha[k+1]_2 + \mu[k]_2, & \text{if } [j]_3 = 1, \\ \gamma[k+1]_2 + \lambda[k]_2, & \text{if } [j]_3 = 2, \end{cases} \tag{36}$$
$$\Phi_3^{(iii)}(j,k) = \begin{cases} \gamma[k+1]_2 + \mu[k]_2, & \text{if } [j]_3 = 0, \\ \beta[k+1]_2 + \lambda[k]_2, & \text{if } [j]_3 = 1, \\ \alpha[k+1]_2 + \kappa[k]_2, & \text{if } [j]_3 = 2. \end{cases} \tag{37}$$

From Eqs. (29)-(37), it is easy to see that

$$\Phi_m^{(i)} \neq \Phi_m^{(i)}(j) \tag{38}$$
$$\Phi_m^{(ii)}(j,k) = \Phi_m^{(ii)}(j \pm 2, k), \tag{39}$$
$$\Phi_m^{(iii)}(j,k) = \Phi_m^{(iii)}(j \pm 3, k). \tag{40}$$

The ten possible formulations for the honeycomb SQW

Config. A	Config. B	Config. C	Config. D	Config. E	Config. F
$\alpha = \lambda$	$\alpha = \mu$	$\alpha = \kappa$	$\alpha = \lambda$	$\alpha = \mu$	$\alpha = \kappa$
$\beta = \kappa$	$\beta = \lambda$	$\beta = \mu$	$\beta = \mu$	$\beta = \kappa$	$\beta = \lambda$
$\gamma = \mu$	$\gamma = \kappa$	$\gamma = \lambda$	$\gamma = \kappa$	$\gamma = \lambda$	$\gamma = \mu$

Table 1: The six possible configuratons for the lattice labeling, depending on the relations between the sets $\{\alpha, \beta, \gamma\}$ and $\{\lambda, \kappa, \mu\}$ in Eq. (28).

For each different manner $\Phi_m(j,k)$ can be constructed — (i), (ii), or (iii) — one does not not loose any generality by assuming that the sets $\{\alpha, \beta, \gamma\}$ and $\{\lambda, \kappa, \mu\}$ in Eq. (28) span the same numerical values. So, we have in total six possible lattice labeling, constituting the configurations A—F shown in Tab. 1. Furthermore, for the distributions (i) [Eqs. (29)-(31)], (ii) [Eqs. (32)-(34)], and (iii) [Eqs. (35)-(37)], these configurations are represented, respectively, in Figs. 10, 12, and 14.

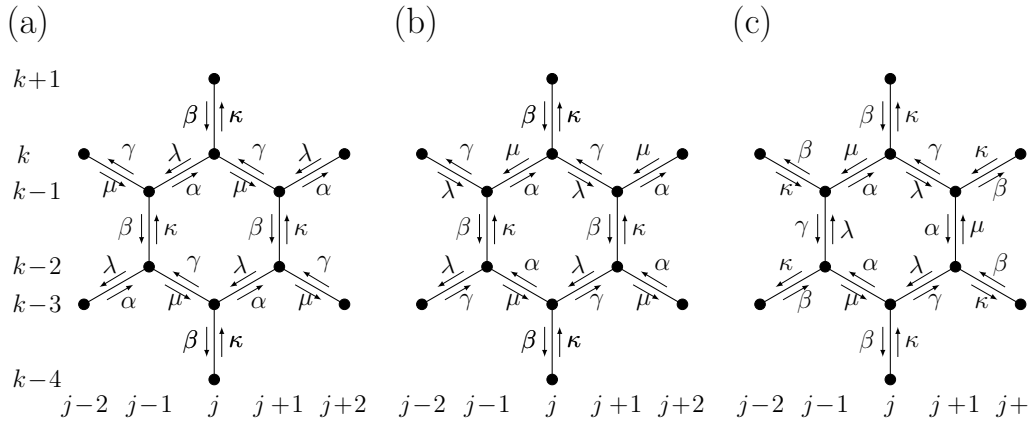

Figure 9: For the *basic segment* of the honeycomb lattice, it is illustrated the three possible ways to ascribe values for the topological directional function $\Phi_m(j,k)$, labeled as: (a) distribution (i), (b) distribution (ii), (c) distribution (iii).

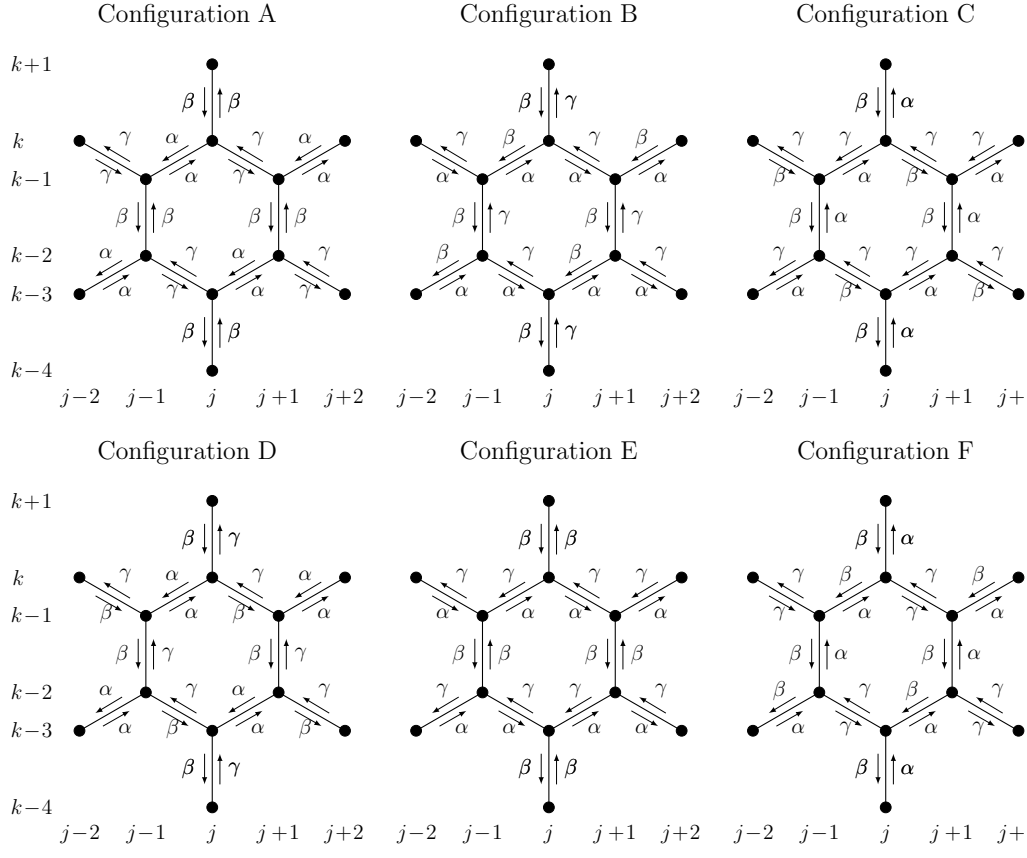

Figure 10: For the distribution (i), the six possible configurations (Tab. 1) of $\Phi_m(j,k)$.

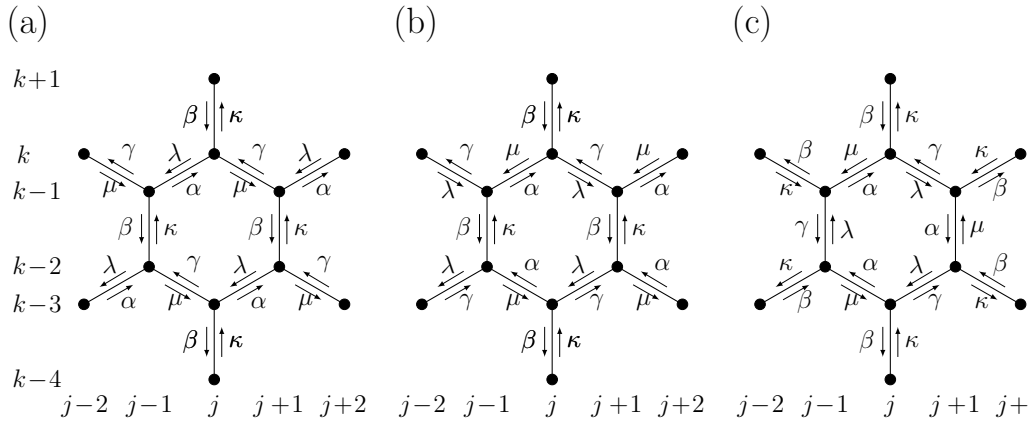

Figure 11: For the *basic segment* of the honeycomb lattice, it is illustrated the three possible ways to ascribe values for the topological directional function $\Phi_m(j,k)$, labeled as: (a) distribution (i), (b) distribution (ii), (c) distribution (iii).

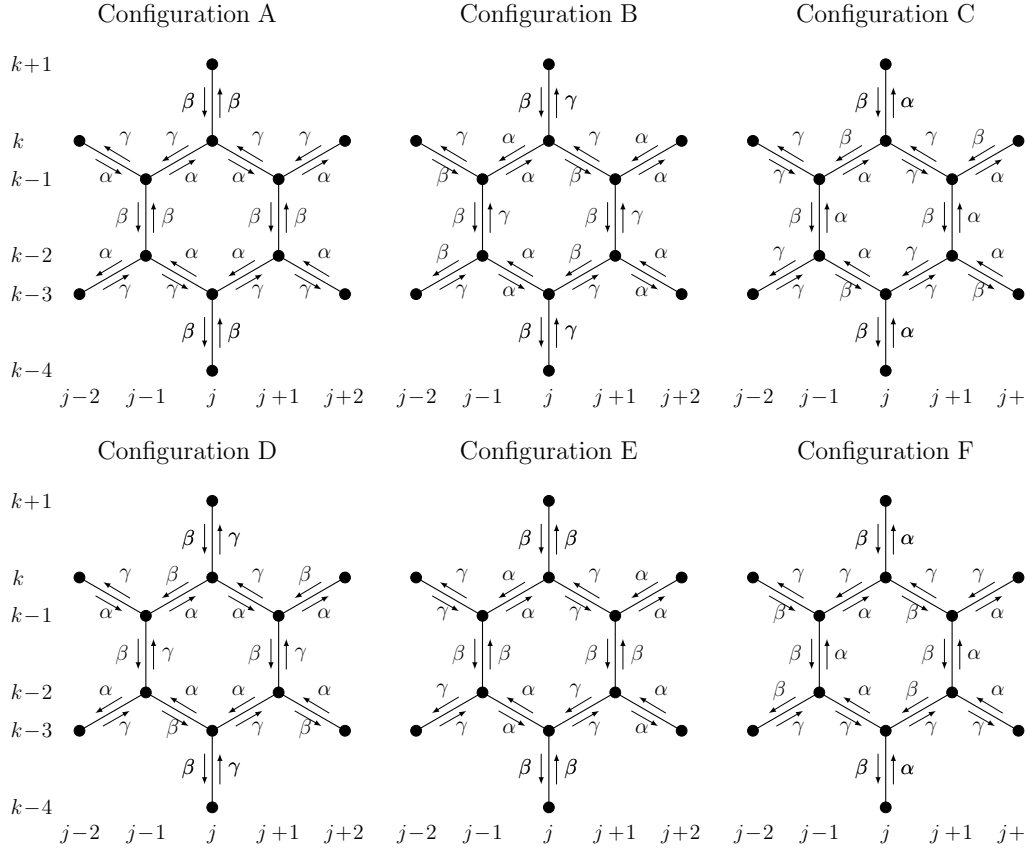

Figure 12: The same as in Fig. 10, but for the distribution (ii).

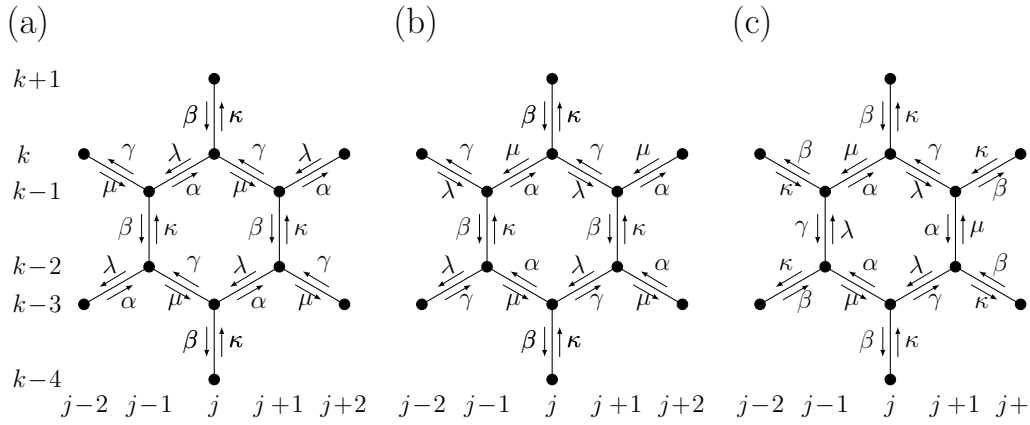

Figure 13: For the *basic segment* of the honeycomb lattice, it is illustrated the three possible ways to ascribe values for the topological directional function $\Phi_m(j,k)$, labeled as: (a) distribution (i), (b) distribution (ii), (c) distribution (iii).

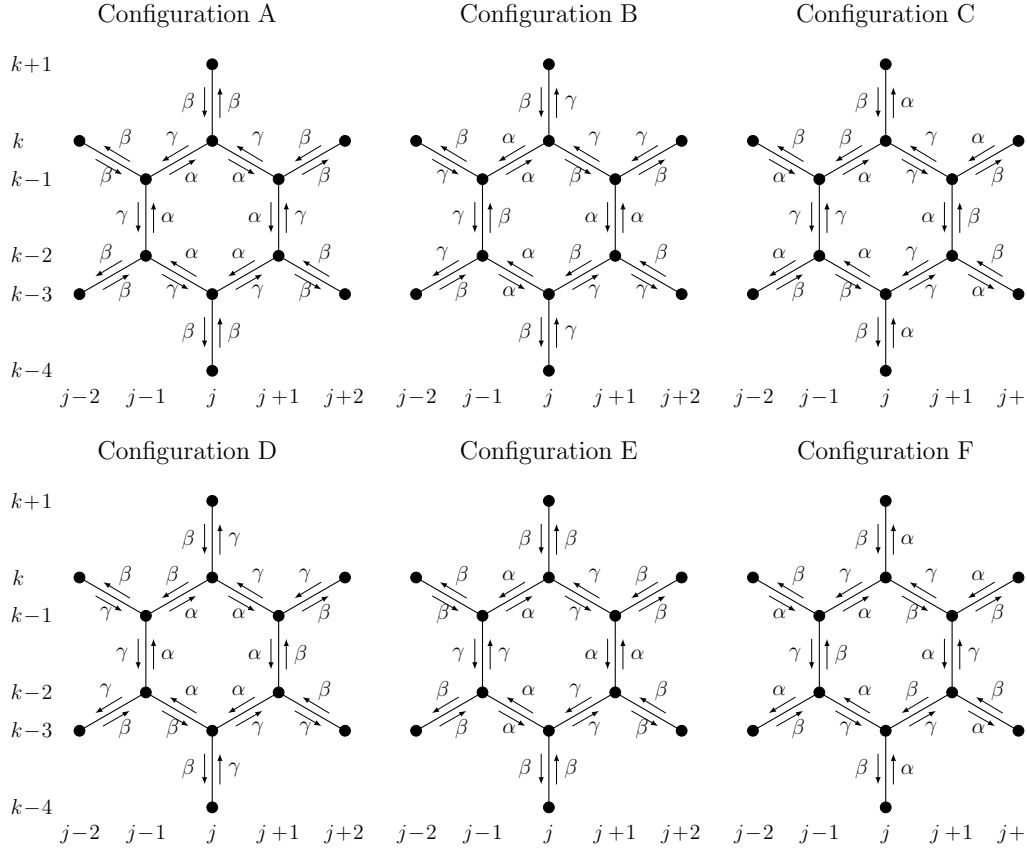

Figure 14: The same as in Fig. 10, but for the distribution (iii).

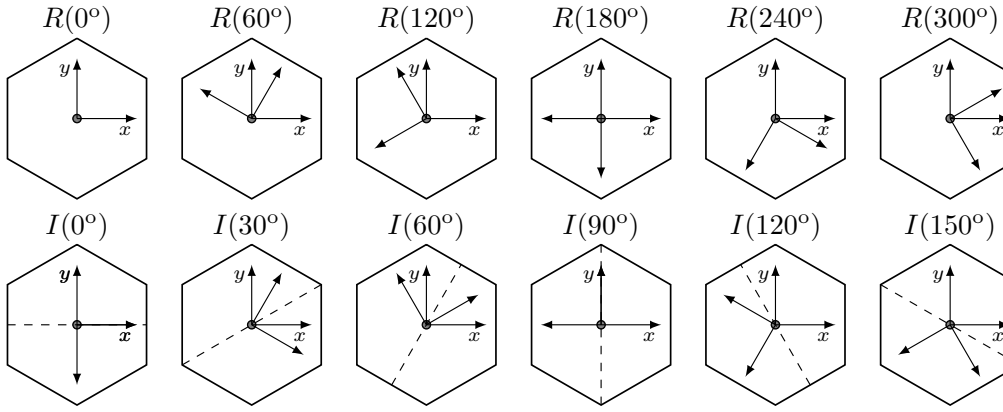

Figure 15: The symmetries of rotations $R(\cdot)$ and inversions $I(\cdot)$ of the hexagonal lattice.

But the honeycomb can be represented as a two-dimensional triangular Bravais lattices with two-point basis. Thus, it is invariant by rotations of 0^o, 60^o, 120^o, 180^o, 240^o and 300^o, and by inversions (reflections) of 0^o, 30^o, 60^o, 90^o, 120^o and 150^o, Fig. 15. Hence, there exist configurations in Figs. 10–14 that are equivalent as a consequence of some of these symmetries, Tab. 2, becoming explicit when one considers proper relabeling of $\{\alpha, \beta, \gamma\}$ (see below).

Distribution	Symmetry
(i)	A
	B $\to$ C: $R(60^o)$, $R(180^o)$, $R(300^o)$, $I(30^o)$, $I(90^o)$, $I(150^o)$
	C $\to$ B: $R(60^o)$, $R(180^o)$, $R(300^o)$, $I(30^o)$, $I(90^o)$, $I(150^o)$
	D $\to$ E: $R(60^o)$, $R(240^o)$, $I(60^o)$, $I(150^o)$
	D $\to$ F: $R(120^o)$, $R(300^o)$, $I(0^o)$, $I(90^o)$
	E $\to$ D: $R(120^o)$, $R(300^o)$, $I(60^o)$, $I(150^o)$
	E $\to$ F: $R(60^o)$, $R(240^o)$, $I(30^o)$, $I(120^o)$
	F $\to$ D: $R(60^o)$, $R(240^o)$, $I(0^o)$, $I(90^o)$
	F $\to$ E: $R(120^o)$, $R(300^o)$, $I(30^o)$, $I(120^o)$
(ii)	A
	B $\to$ C: $R(180^o)$, $I(90^o)$
	C $\to$ B: $R(180^o)$, $I(90^o)$
	D $\to$ F: $I(0^o)$, $I(90^o)$
	E
	F $\to$ D: $I(0^o)$, $I(90^o)$
(iii)	A
	B $\to$ C: $R(60^o)$, $R(180^o)$, $R(300^o)$, $I(30^o)$, $I(90^o)$, $I(150^o)$
	C $\to$ B: $R(60^o)$, $R(180^o)$, $R(300^o)$, $I(30^o)$, $I(90^o)$, $I(150^o)$
	D $\to$ F: $I(0^o)$, $I(30^o)$, $I(60^o)$, $I(90^o)$, $I(120^o)$, $I(150^o)$
	E
	F $\to$ D: $I(0^o)$, $I(30^o)$, $I(60^o)$, $I(90^o)$, $I(120^o)$, $I(150^o)$

Table 2: For each Φ_m distribution of values (i), (ii), (iii), the configurations — see, respectively, Figs. 10, 12, 14 — which are equilvalent due to the lattice symmetries (and becoming manifest from appropriate relabeling of $\{\alpha, \beta, \gamma\}$, as exemplified in the main text).

SQW Formulation	Distribution	Equivalent Configurations
1	(i)	A*
2	(i)	B* $\sim$ C
3	(i)	D $\sim$ E* $\sim$ F
4	(ii)	A*
5	(ii)	B* $\sim$ C
6	(ii)	D* $\sim$ F
7	(ii)	E*
8	(iii)	A* $\sim$ B $\sim$ C
9	(iii)	D* $\sim$ F
10	(iii)	E*

Table 3: The ten distinct formulations for SQWs in the honeycomb lattice. For each distribution (i)–(iii) of σ values, it is indicated which configurations are equivalent ($\sim$). That with "$*$" will be taken as the one representing the others equivalent configurations.

Putting all these results together, we finally concluded that there are in total ten distinct self-consistent ways of distributing the σ values (by means of the topological directional function Φ) in the honeycomb lattice, Tab. 3. Each one leading to a distinct formulation for the SQW.

Finally, the distribution of the σ values for each formulation l ($l = 1, \ldots, 10$) are given by $\Phi_m^{(l)}(j,k)$, reading

$$\Phi_1^{(1)}(j,k) = \alpha, \tag{41}$$
$$\Phi_2^{(1)}(j,k) = \beta, \tag{42}$$
$$\Phi_3^{(1)}(j,k) = \gamma, \tag{43}$$

$$\Phi_1^{(2)}(j,k) = \alpha[k+1]_2 + \beta[k]_2, \tag{44}$$
$$\Phi_2^{(2)}(j,k) = \beta[k+1]_2 + \gamma[k]_2, \tag{45}$$
$$\Phi_3^{(2)}(j,k) = \gamma[k+1]_2 + \alpha[k]_2, \tag{46}$$

$$\Phi_1^{(3)}(j,k) = \alpha[k+1]_2 + \gamma[k]_2, \tag{47}$$
$$\Phi_2^{(3)}(j,k) = \beta, \tag{48}$$
$$\Phi_3^{(3)}(j,k) = \gamma[k+1]_2 + \alpha[k]_2, \tag{49}$$

$$\Phi_1^{(4)}(j,k) = \begin{cases} \alpha, & \text{if } [j]_2 = 0, \\ \gamma, & \text{if } [j]_2 = 1, \end{cases} \tag{50}$$
$$\Phi_2^{(4)}(j,k) = \beta, \tag{51}$$
$$\Phi_3^{(4)}(j,k) = \begin{cases} \gamma[k+1]_2, & \text{if } [j]_2 = 0, \\ \alpha[k+1]_2, & \text{if } [j]_2 = 1, \end{cases} \tag{52}$$

$$\Phi_1^{(5)}(j,k) = \begin{cases} \alpha[k+1]_2 + \beta[k]_2, & \text{if } [j]_2 = 0, \\ \gamma[k+1]_2 + \alpha[k]_2, & \text{if } [j]_2 = 1, \end{cases} \tag{53}$$
$$\Phi_2^{(5)}(j,k) = \beta[k+1]_2 + \gamma[k]_2, \tag{54}$$
$$\Phi_3^{(5)}(j,k) = \begin{cases} \gamma[k+1]_2 + \alpha[k]_2, & \text{if } [j]_2 = 0, \\ \alpha[k+1]_2 + \beta[k]_2, & \text{if } [j]_2 = 1, \end{cases} \tag{55}$$

$$\Phi_1^{(6)}(j,k) = \begin{cases} \alpha, & \text{if } [j]_2 = 0, \\ \gamma[k+1]_2 + \beta[k]_2, & \text{if } [j]_2 = 1, \end{cases} \tag{56}$$

$$\Phi_2^{(6)}(j,k) = \beta[k+1]_2 + \gamma[k]_2, \tag{57}$$

$$\Phi_3^{(6)}(j,k) = \begin{cases} \gamma[k+1]_2 + \beta[k]_2, & \text{if } [j]_2 = 0, \\ \alpha[k+1]_2, & \text{if } [j]_2 = 1, \end{cases} \tag{58}$$

$$\Phi_1^{(7)}(j,k) = \begin{cases} \alpha[k+1]_2 + \gamma[k]_2, & \text{if } [j]_2 = 0, \\ \gamma[k+1]_2 + \alpha[k]_2, & \text{if } [j]_2 = 1, \end{cases} \tag{59}$$

$$\Phi_2^{(7)}(j,k) = \beta[k+1]_2, \tag{60}$$

$$\Phi_3^{(7)}(j,k) = \begin{cases} \gamma[k+1]_2 + \alpha[k]_2, & \text{if } [j]_2 = 0, \\ \alpha[k+1]_2 + \gamma[k]_2, & \text{if } [j]_2 = 1, \end{cases} \tag{61}$$

$$\Phi_1^{(8)}(j,k) = \begin{cases} \alpha, & \text{if } [j]_3 = 0, \\ \gamma[k+1]_2 + \beta[k]_2, & \text{if } [j]_3 = 1, \\ \beta[k+1]_2 + \gamma[k]_2, & \text{if } [j]_3 = 2, \end{cases} \tag{62}$$

$$\Phi_2^{(8)}(j,k) = \begin{cases} \beta, & \text{if } [j]_3 = 0, \\ \alpha[k+1]_2 + \gamma[k]_2, & \text{if } [j]_3 = 1, \\ \gamma[k+1]_2 + \alpha[k]_2, & \text{if } [j]_3 = 2, \end{cases} \tag{63}$$

$$\Phi_3^{(8)}(j,k) = \begin{cases} \gamma, & \text{if } [j]_3 = 0, \\ \beta[k+1]_2 + \alpha[k]_2, & \text{if } [j]_3 = 1, \\ \alpha[k+1]_2 + \beta[k]_2, & \text{if } [j]_3 = 2, \end{cases} \tag{64}$$

$$\Phi_1^{(9)}(j,k) = \begin{cases} \alpha, & \text{if } [j]_3 = 0, \\ \gamma, & \text{if } [j]_3 = 1, \\ \beta, & \text{if } [j]_3 = 2, \end{cases} \tag{65}$$

$$\Phi_2^{(9)}(j,k) = \begin{cases} \beta[k+1]_2 + \gamma[k]_2, & \text{if } [j]_3 = 0, \\ \alpha[k+1]_2 + \beta[k]_2, & \text{if } [j]_3 = 1, \\ \gamma[k+1]_2 + \alpha[k]_2, & \text{if } [j]_3 = 2, \end{cases} \tag{66}$$

$$\Phi_3^{(9)}(j,k) = \begin{cases} \gamma[k+1]_2 + \beta[k]_2, & \text{if } [j]_3 = 0, \\ \beta[k+1]_2 + \alpha[k]_2, & \text{if } [j]_3 = 1, \\ \alpha[k+1]_2 + \gamma[k]_2, & \text{if } [j]_3 = 2, \end{cases} \tag{67}$$

$$\Phi_1^{(10)}(j,k) = \begin{cases} \alpha[k+1]_2 + \gamma[k]_2, & \text{if } [j]_3 = 0, \\ \gamma[k+1]_2 + \beta[k]_2, & \text{if } [j]_3 = 1, \\ \beta[k+1]_2 + \alpha[k]_2, & \text{if } [j]_3 = 2, \end{cases} \tag{68}$$

$$\Phi_2^{(10)}(j,k) = \begin{cases} \beta, & \text{if } [j]_3 = 0, \\ \alpha, & \text{if } [j]_3 = 1, \\ \gamma, & \text{if } [j]_3 = 2, \end{cases} \tag{69}$$

$$\Phi_3^{(10)}(j,k) = \begin{cases} \gamma[k+1]_2 + \alpha[k]_2, & \text{if } [j]_3 = 0, \\ \beta[k+1]_2 + \gamma[k]_2, & \text{if } [j]_3 = 1, \\ \alpha[k+1]_2 + \beta[k]_2, & \text{if } [j]_3 = 2. \end{cases} \tag{70}$$

In the Figs. 16 and 17 we show the σ values distributions, Eqs. (41)–(70), for all the possible ten distinc formulations.

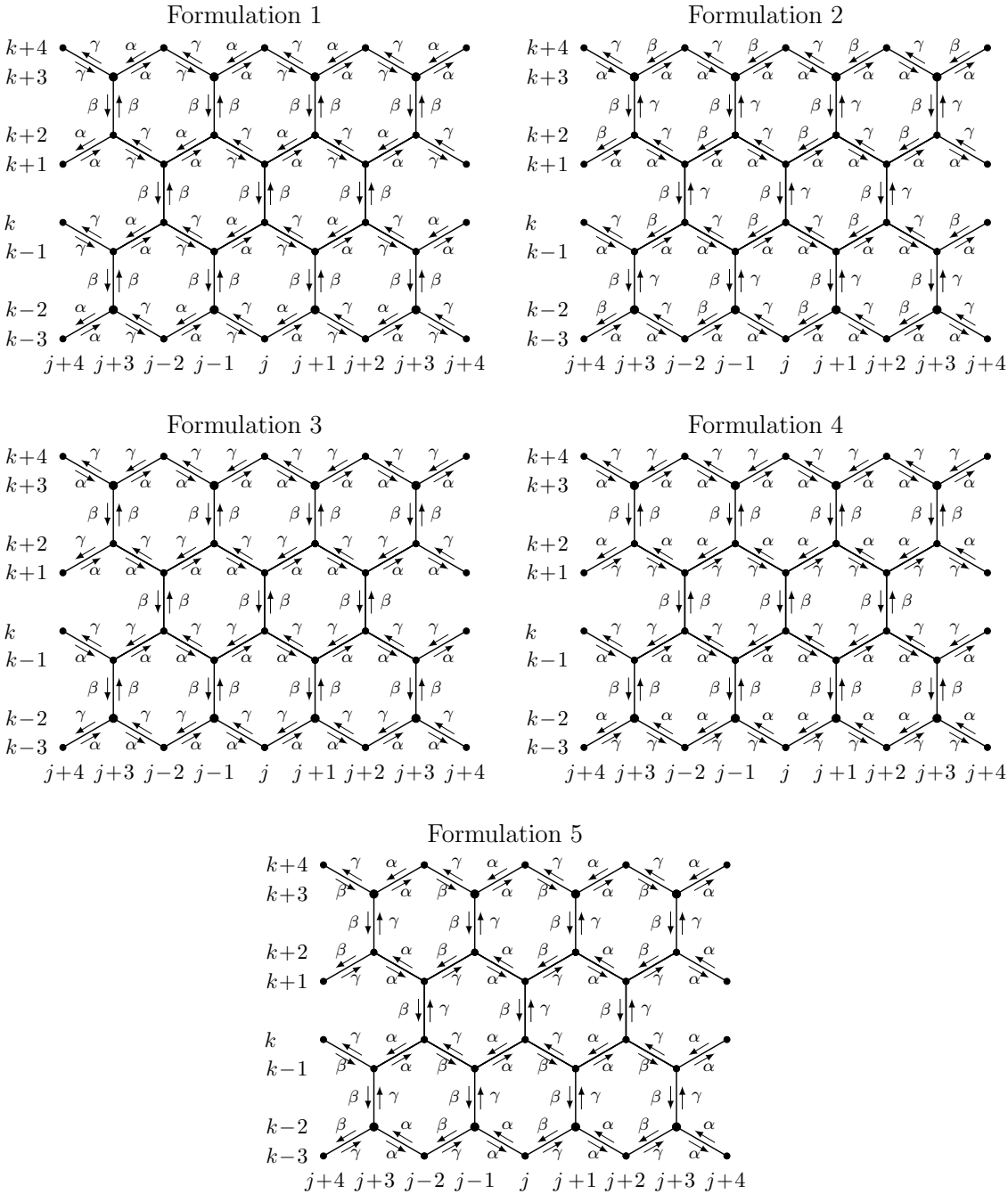

Figure 16: Distribution of the σ values in the honeycomb lattice for the distinct SQWs formulations 1 to 5.

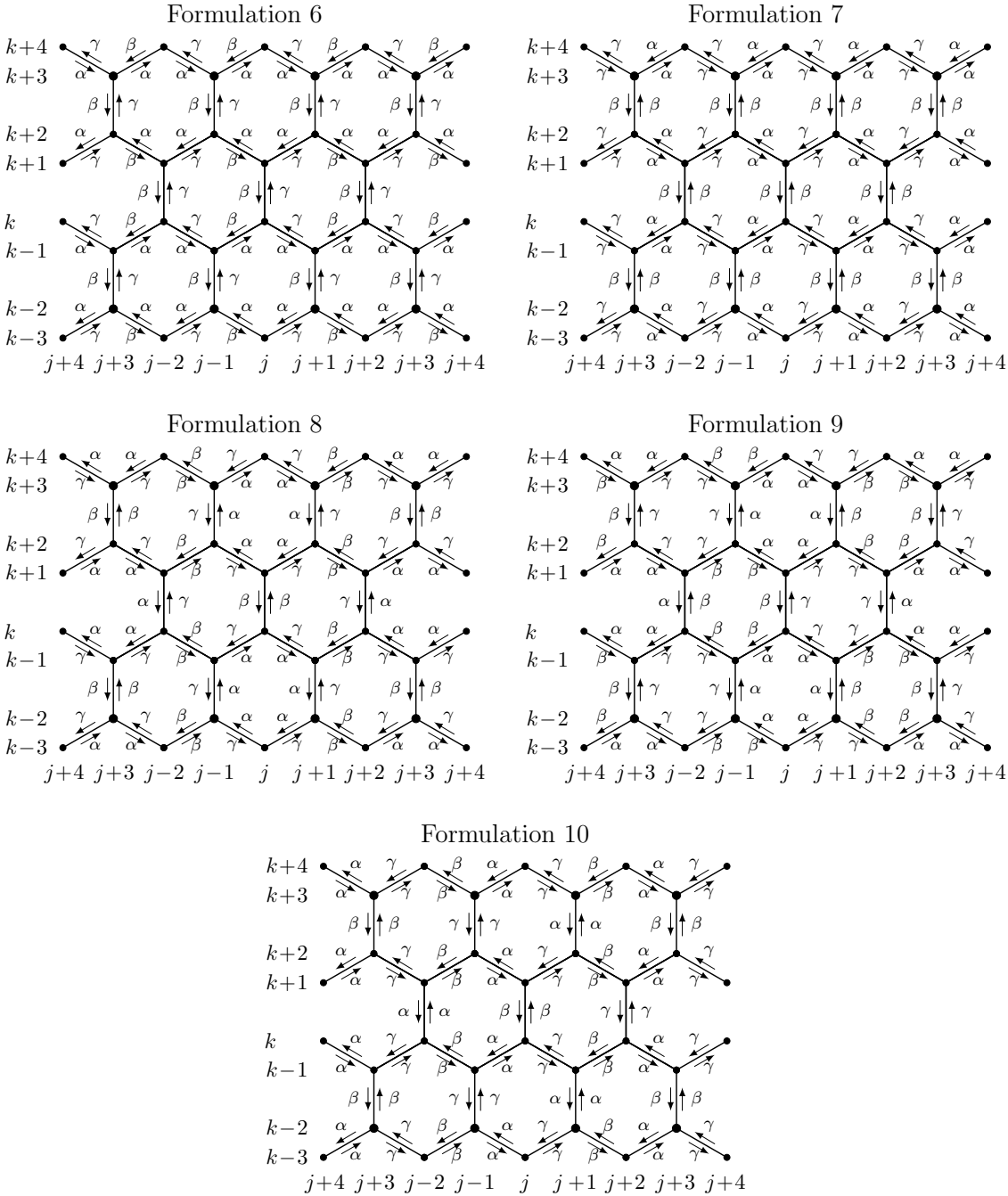

Figure 17: Distribution of the σ values in the honeycomb lattice for the distinct SQWs formulations 6 to 10.

Finally, we recall that one can choose the values of σ, i.e., the values for $\{\alpha, \beta, \gamma\}$, in a complete arbitrary fashion. But a proper choice can enormously simplify the notation. For example, in formulation 1, Fig. 16, if we choose $\alpha = 1$, $\beta = 2$, $\gamma = 3$, the Eqs. (41)-(43) reduce to $\Phi_m^{(1)} = m$, with $m = 1, 2, 3$. In formulation 3, Fig. 16, for $\alpha = +1$, $\beta = 0$ and $\gamma = -1$, Eqs. (47)-(49) reduce to $\Phi_m^{(3)}(j,k) = (2-m)([k+1]_2 - [k]_2)$. The formulation 9, Fig. 17, corresponds to the honeycomb SQW model of [**?**] by setting $\alpha = 2$, $\beta = 1$, $\gamma = 0$. So, in this case the Eqs. (65)-(67) reduce to

$$\Phi_1^{(9)}(j,k) = [j-1]_3, \tag{71}$$

$$\Phi_2^{(9)}(j,k) = [j+1]_3[k+1]_2 + [j]_3[k]_2, \tag{72}$$

$$\Phi_3^{(9)}(j,k) = [j]_3[k+1]_2 + [j+1]_3[k]_2. \tag{73}$$

Applications: (1) The concept of 'characteristic paths'

A helpful concept to portray certain properties of a QW formulation — and which is close to the idea of classical RWs — is that of 'characteristic paths', first introduced in J. Phys. A **46**, 165302 (2013). For a given σ and arbitrary (j_0, k_0), suppose the state $|\psi_1\rangle = \hat{U}|\sigma, j_0, k_0\rangle$. According to Eq. (14), in general terms we can write $|\psi_1\rangle = \sum_{\sigma'} c_{\sigma'}|\sigma', j_{\sigma'}, k_{\sigma'}\rangle$ with $(j_{\sigma'}, k_{\sigma'})$ properly related to the direction quantum number σ' and the c's representing the corresponding $\Gamma^{(j_0,k_0)}$ elements. But note that one of these σ' values is exaclty σ. For such $\sigma' = \sigma$ we denote $j_{\sigma'=\sigma} = j_1$ and $k_{\sigma'=\sigma} = k_1$. Next, we consider $|\sigma, j_1, k_1\rangle$ and calculate $|\psi_2\rangle = \hat{U}|\sigma, j_1, k_1\rangle = \sum_{\sigma''} c_{\sigma''}|\sigma'', j_{\sigma''}, k_{\sigma''}\rangle$, selecting (from the sum over σ'' spanning $|\psi_2\rangle$) the basis state $|\sigma, j_2, k_2\rangle$. Then, we compute $|\psi_3\rangle = \hat{U}|\sigma, j_2, k_2\rangle = \sum_{\sigma'''} c_{\sigma'''}|\sigma''', j_{\sigma'''}, k_{\sigma'''}\rangle$, this time selecting $|\sigma, j_3, k_3\rangle$, and so on and so forth. From the procedure, we generate the sequence

$$|\sigma, j_0, k_0\rangle \xrightarrow{\hat{U}} |\sigma, j_1, k_1\rangle \xrightarrow{\hat{U}} |\sigma, j_2, k_2\rangle \xrightarrow{\hat{U}} |\sigma, j_3, k_3\rangle \ldots . \qquad (74)$$

The lattice bonds and directions associated to the quantum numbers of these succession of basis states form a "trajectory", being the characteristic path σ of the formulation defined by $\hat{U}$.

In Tab. 4 we list the qualitative shapes of the characteristic paths for the honeycomb ten possible SQW formulations. Such trajectory shapes can be identified in Figs. 16 and 17 by tracking the succession of bonds which have a same directional quantum number σ. We also depict all these paths in Figs. 18, 19, and 20. We clearly see that we can have either confinement (as back and forth scattering in a single bond or a loop-like movement along a single lattice hexagon) Fig. 18, or a balistic-like diffusion (as zigzag or armchair types of movement patterns) Fig. 19. In fact, certain formulations allow both kind of characteristic paths, Fig. 20.

Formulation	$\sigma = \alpha$	$\sigma = \beta$	$\sigma = \gamma$
1	back and forth	back and forth	back and forth
2	zigzag	zigzag	zigzag
3	zigzag	back and forth	zigzag
4	zigzag	back and forth	zigzag
5	back and forth	armchair	armchair
6	zigzag	armchair	armchair
7	back and forth	back and forth	back and forth
8	loop	back and forth	loop
9	loop	loop	loop
10	back and forth	back and forth	back and forth

Table 4: The qualitative trajectories shapes of the characteristic paths σ for the honeycomb SQWs ten formulations.

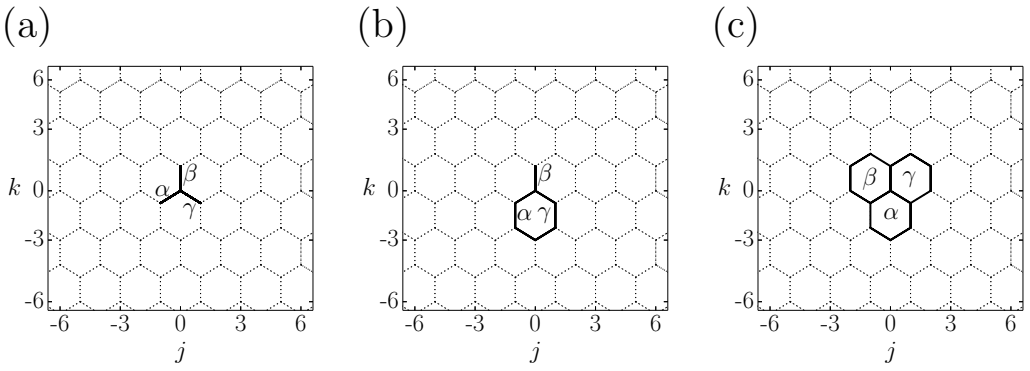

Figure 18: Illustrative examples of characteristic paths $\sigma = \alpha, \beta, \gamma$ for some SQW formulations. (a) All such paths are confining back and forth scattering along a single bond in formulations 1, 7, 10. (b) For formulation 8, the characteristic paths are also confining, either as back and forth scattering, $\sigma = \beta$, or as closed loops trajectories, clockwise for $\sigma = \alpha$ and anticlockwise for $\sigma = \gamma$. (c) For formulation 9, all the characteristic paths are clockwise closed loops.

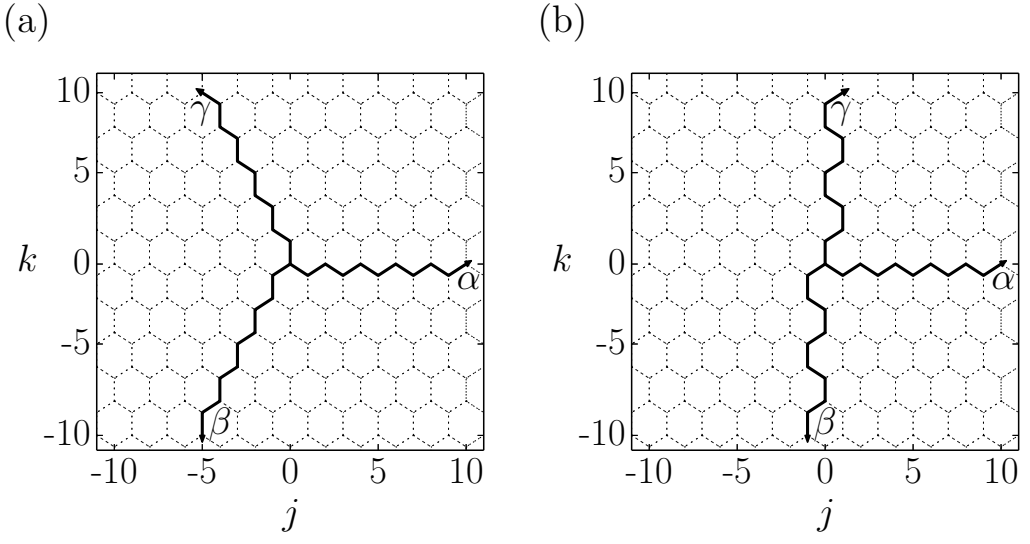

Figure 19: The characteristics paths $\sigma = \alpha, \beta, \gamma$ for the formulations (a) 2 and (b) 6. In these cases, the trajectories are balistic-like, following either zigzag or armchair shapes.

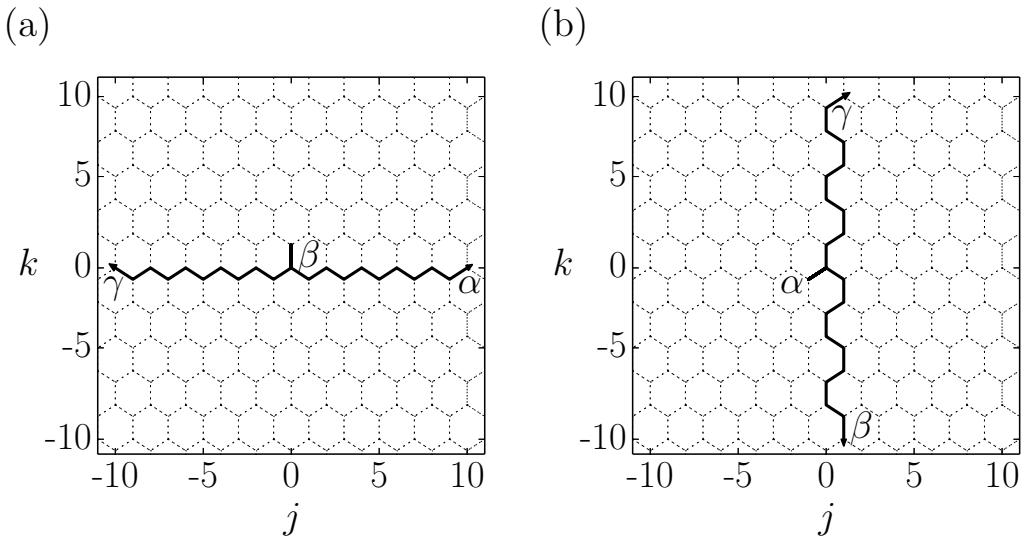

Figure 20: The characteristics paths $\sigma = \alpha, \beta, \gamma$ for the formulations (a) 3, 4 and (b) 5. For these formulations, the trajectories can be either confining (of back and forth type) or balistic-like (either zigzag in (a) and armchair in (b)).

Note that due to the general way the scattering matrix Γ is defined, Eq. (18), the probabilistic occurence of characteristic paths is governed by the main diagonal elements of Γ (which may represent reflection or transmission coeficients depending on the formulation). Analyzing the Figs. (16)-(17), one finds that the connection between the Γ elements and the quantum amplitudes associated to the $\sigma \to \sigma$ transitions are the following:

- formulations 1, 7, 10

$$\Gamma_{\alpha\alpha}^{(j,k)} = r_{\alpha\alpha}^{(j,k)}, \;\; \Gamma_{\beta\beta}^{(j,k)} = r_{\beta\beta}^{(j,k)}, \;\; \Gamma_{\gamma\gamma}^{(j,k)} = r_{\gamma\gamma}^{(j,k)}; \qquad (75)$$

- formulations 2, 6, 9

$$\Gamma_{\alpha\alpha}^{(j,k)} = t_{\alpha\alpha}^{(j,k)}, \;\; \Gamma_{\beta\beta}^{(j,k)} = t_{\beta\beta}^{(j,k)}, \;\; \Gamma_{\gamma\gamma}^{(j,k)} = t_{\gamma\gamma}^{(j,k)}; \qquad (76)$$

- formulations 3, 4, 8

$$\Gamma_{\alpha\alpha}^{(j,k)} = t_{\alpha\alpha}^{(j,k)}, \;\; \Gamma_{\beta\beta}^{(j,k)} = r_{\beta\beta}^{(j,k)}, \;\; \Gamma_{\gamma\gamma}^{(j,k)} = t_{\gamma\gamma}^{(j,k)}; \qquad (77)$$

- formulation 5

$$\Gamma_{\alpha\alpha}^{(j,k)} = r_{\alpha\alpha}^{(j,k)}, \;\; \Gamma_{\beta\beta}^{(j,k)} = t_{\beta\beta}^{(j,k)}, \;\; \Gamma_{\gamma\gamma}^{(j,k)} = t_{\gamma\gamma}^{(j,k)}. \qquad (78)$$

So, in the quantum evolution the (partial) apperance of probability patterns associated to the characteristic paths will depend on the particular scattering matrix Γ chosen, as numerically illustrated next.

Applications: (2) Numerical Evolution

To illustrate the previous results, in the following we present some numerical calculations for the time evolution of SQWs on the honeycomb lattice. We consider the ten formulations and assume explicit forms for the scattering matrices $\Gamma^{(j,k)} = \Gamma$, $\forall$ (j,k). Also, for all the examples we take $|\psi_0\rangle$ as

$$|\psi_0\rangle = \frac{1}{\sqrt{3}} \left(|\alpha, 0, 0\rangle + |\beta, 0, 0\rangle + |\gamma, 0, 0\rangle \right). \tag{79}$$

Hence the initial state is not biased towards any direction.

The scattering matrix Γ as the Discrete Fourier Transform (DFT)

As a first concrete case, we set Γ as

$$\Gamma_{DFT} = \frac{1}{\sqrt{3}} \begin{pmatrix} 1 & 1 & 1 \\ 1 & \exp[-2i\pi/3] & \exp[+2i\pi/3] \\ 1 & \exp[+2i\pi/3] & \exp[-2i\pi/3] \end{pmatrix}. \qquad (80)$$

Observe it is "unbiased" since $|\Gamma_{\sigma''\sigma';DFT}|^2 = 1/3$ for any σ'' and σ'. Further

$$\sum_{\sigma''} \Gamma_{\sigma''\alpha;DFT} = \sum_{\sigma''} \Gamma_{\alpha\sigma'';DFT} = \sqrt{3},$$
$$\sum_{\sigma''} \Gamma_{\sigma''\sigma';DFT} = \sum_{\sigma''} \Gamma_{\sigma'\sigma'';DFT} = 0 \quad \text{for} \quad \sigma' \neq \alpha, \qquad (81)$$

For definiteness, unless otherwise explicitly mentioned we evolve the corresponding ten formulations a total of $n = 10^3$ time steps and look at the quantum spatial probability distributions $P_{n=10^3}(j,k)$, Eq. (23). For comparison, we also consider a classical RW, leaving from the origin and having equal probabilities to go to any direction. The classical and quantum cases are shown, respectively, in Figs. 21 and 22. As one can see, in general the SQWs P_n patterns, Fig. 22, are much richier than the classical RW typical Gaussian-like distribution of Fig. 21.

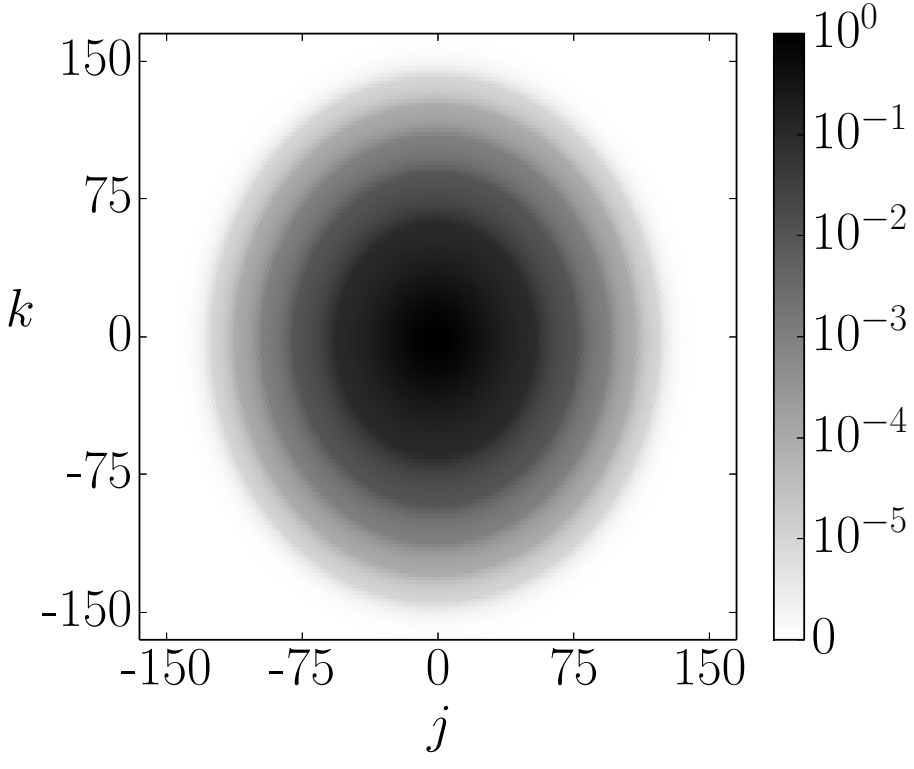

Figure 21: The spatial probability distribution of a typical classical RW leaving from the origin after $n = 10^3$ time steps. The probabilities to go the three possible directions are always the same, each equal to 1/3.

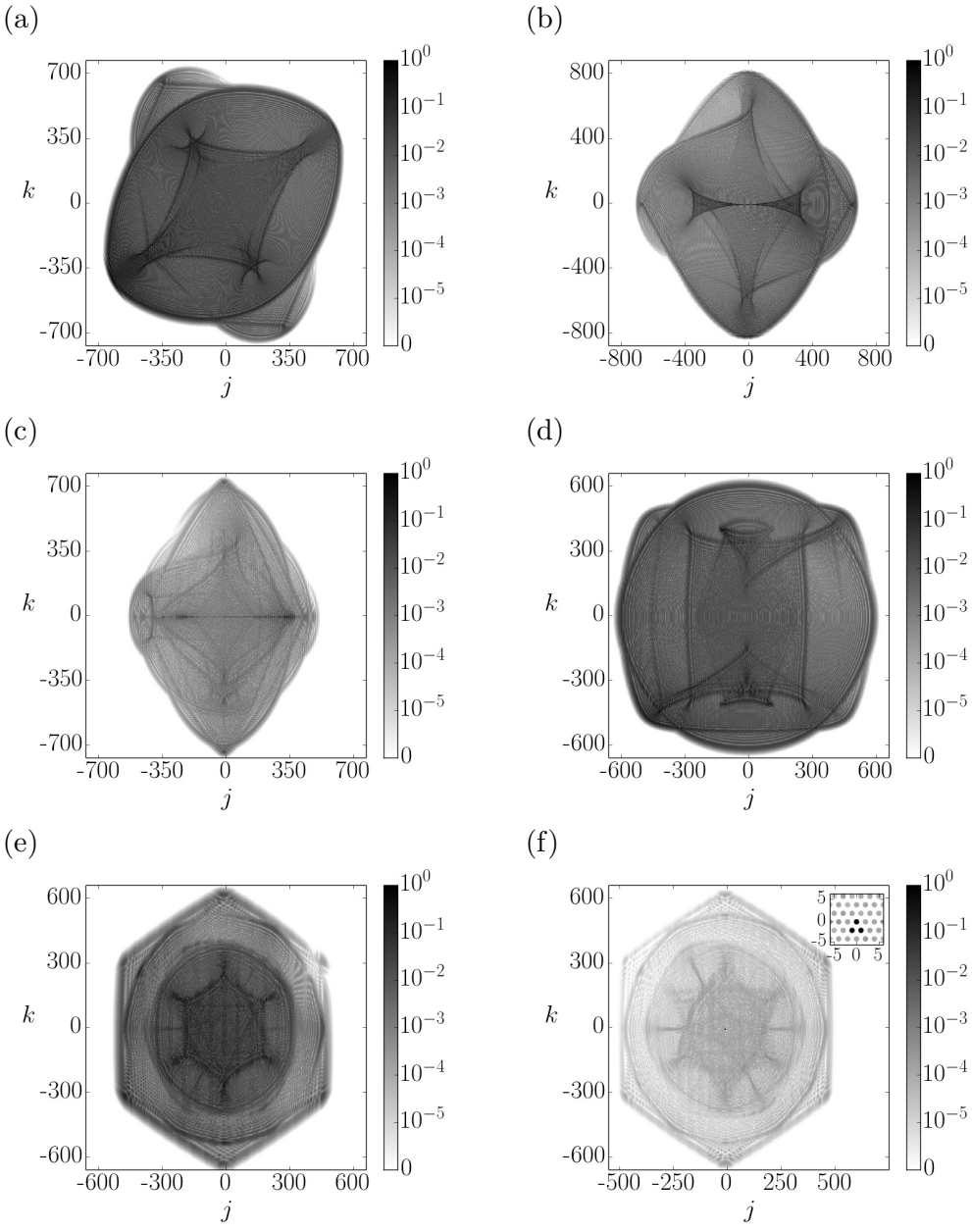

Figure 22: The SQW normalized spatial distribution of probabilities after $n = 10^3$ time steps $P_{n=10^3}(j,k)$, Eq. (23), for the DFT scattering matrix, Eq. (80), and the initial state of Eq. (79). The formulations are: (a) 1, (b) 2 and 3, (c) 4 and 6, (d) 5 and 7, (e) 10, (f) 8 and 9 — the reasons for some formulations to present a same P_n pattern are discussed in the main text. The inset in (f) heighlight the high probability to stay close to the initial bonds (even at large n's) in the case of formulations 8 and 9 and Γ_{DFT}.

An important feature distinguishing usual (i.e., Brownian-like) RWs from the corresponding QWs concerns the mean square displacement $\langle(\Delta r)^2\rangle$, defined as

$$\langle(\Delta r)^2\rangle = \sum_{j,k} P_n(j,k)\, r(j,k)^2 - \left(\sum_{j,k} P_n(j,k,n)\, r(j,k)\right)^2, \tag{82}$$

for the radial distance, from the origin to the site (j,k), given by

$$r(j,k) = \sqrt{x(j)^2 + y(k)^2}, \tag{83}$$

with $x(j)$ and $y(j)$ in Eq. (8). Generally, while for the classical case $\langle(\Delta r)^2\rangle \sim n$, for QWs $\langle(\Delta r)^2\rangle \sim n^2$. The QWs supperdiffusion (in fact ballistic-like behavior) is a consequence of constructive intereference taking place for the longest possible paths in the lattice.

In Fig. 23 we show $\langle(\Delta r)^2\rangle$ versus n for the SQWs ten formulations (with Γ_{DFT}) and for the classical RW (of equal probabilities). To qualitatively understand how the slopes depend on the different formulations, one can inspect Fig. 22 (where $n = 10^3$). For example, among all formulations, 2 and 3 (Fig. 22 (b)) are those presenting a higher overall spread (reaching the farthest sites), thus displaying the faster increasing of $\langle(\Delta r)^2\rangle$ in Fig. 23. Also, although formulation 10 (Fig. 22 (e)) and formulations 8 and 9 (Fig. 22 (f)) have a fairly similar spatial pattern for $P_{n=10^3}$, for the former the probabilities are higher for the more central sites, i.e., for j and k up to 200 (compare the gray scale variation in the center and in the borders of Fig. 22 (e) with that of Fig. 22 (f)). This makes $\langle(\Delta r)^2\rangle(n)|_{\text{formul. 10}} < \langle(\Delta r)^2\rangle(n)|_{\text{formul. 8 and 9}}$.

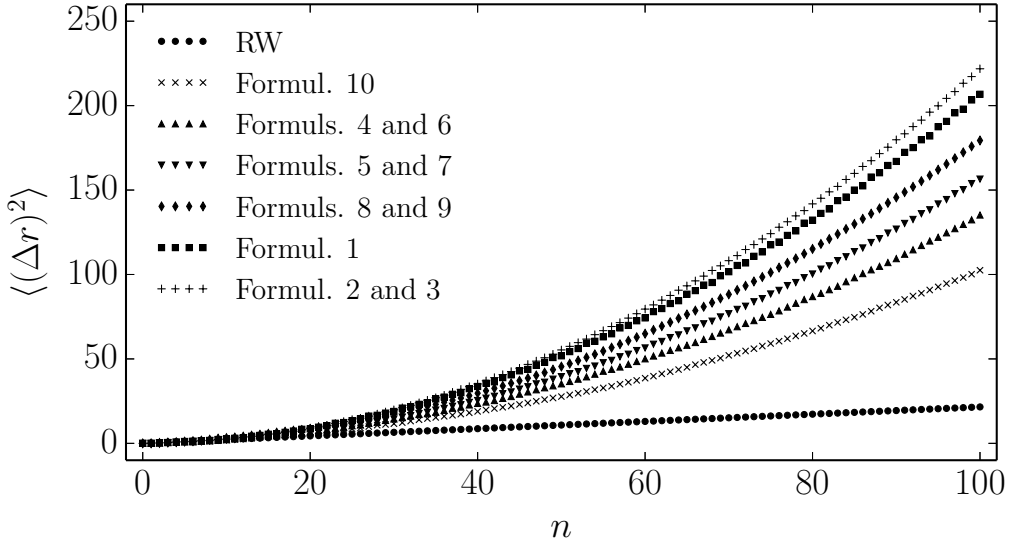

Figure 23: $\langle(\Delta r)^2\rangle$ versus n for the SQW ten formulations using the *DFT* scattering matrix (and for the initial state of Eq. (79)) and for an usual classical RW with the same probability to go to any direction (and leaving from the origin).

Probability patterns, characteristic paths and the choice of Γ

As previously discussed, the concept of characteristic paths (CPs) are associated to some important features of a given SQW construction. Thus, reminding that sequences $\sigma \to \sigma \to \sigma \ldots$ are controlled by the scattering matrix main diagonal, Sec. b, a proper choice of Γ can help to unveil such features. To illustrate this, we consider two distinct Γ's. One is a biased scattering matrix, reading (where $\theta_B = \arccos[1/8]$)

$$\Gamma_B = \frac{2\sqrt{2}}{3}\begin{pmatrix} -\exp[i\theta_B] & 1/4 & 1/4 \\ 1/4 & -\exp[i\theta_B] & 1/4 \\ 1/4 & 1/4 & -\exp[i\theta_B] \end{pmatrix}. \tag{84}$$

The other is the Grover matrix, commonly used in the investigation of QWs (mainly due to its relevance in implementing quantum logic gates), or

$$\Gamma_G = \frac{1}{3}\begin{pmatrix} -1 & 2 & 2 \\ 2 & -1 & 2 \\ 2 & 2 & -1 \end{pmatrix}. \tag{85}$$

Note that (with $\sigma'' \neq \sigma'$)

$$\begin{aligned} |\Gamma_{\sigma\sigma;G}|^2 = 1/9 < |\Gamma_{\sigma\sigma;B}|^2 = 8/9, \\ |\Gamma_{\sigma''\sigma';G}|^2 = 4/9 > |\Gamma_{\sigma''\sigma';B}|^2 = 1/18. \end{aligned} \tag{86}$$

Therefore, in a given time step the transition probability from an eigenstate of directional quantum number σ to another eigenstate with the same σ (so 'following' a CP) is of around 11.11% for Γ_G and around 88.89% for Γ_B. We should thus expect the spatial patterns of $P_n(j,k)$ to better reflect the dynamical trends of CPs for Γ_B than for Γ_G.

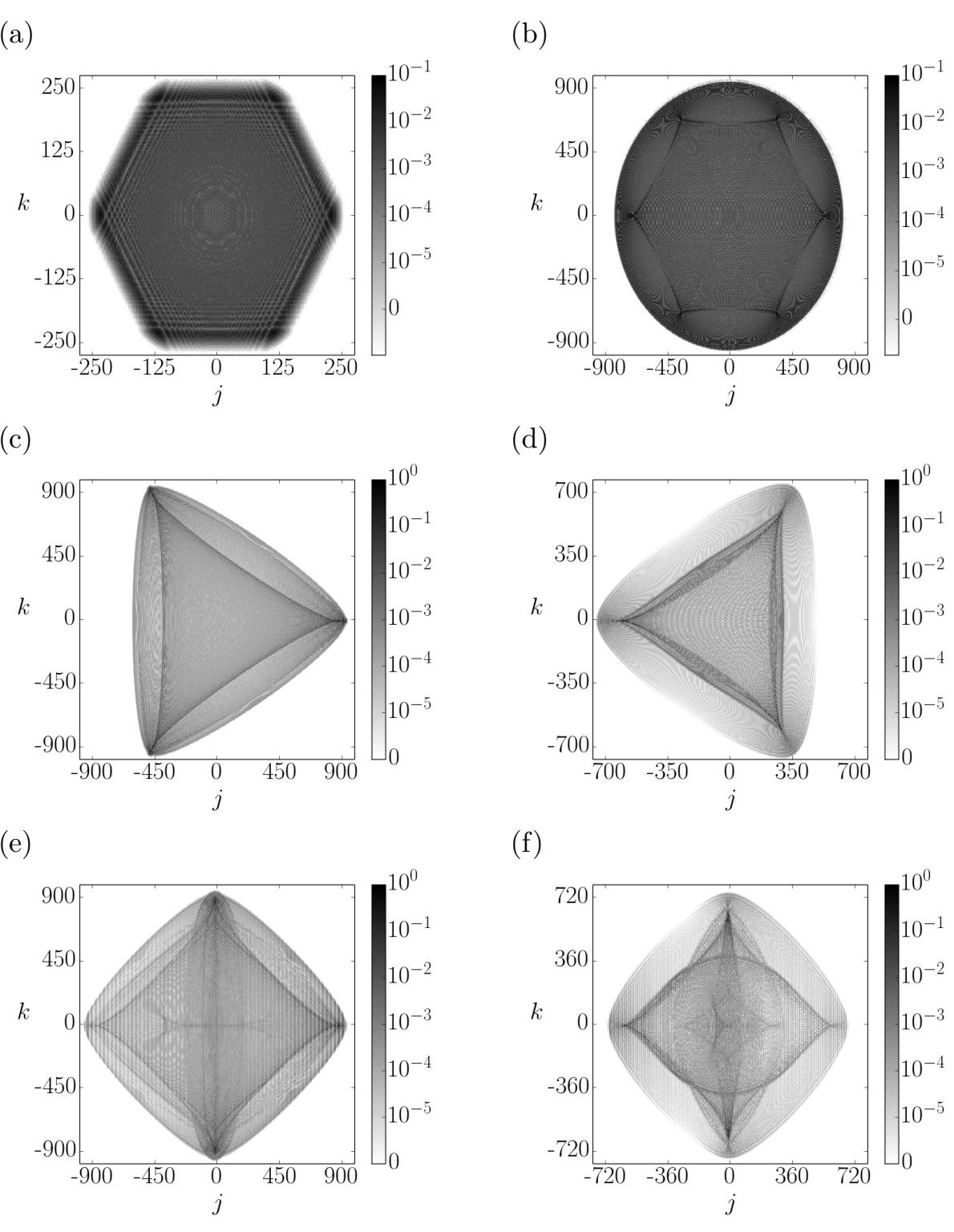

Figure 24: The spatial probability distribution of $P_{n=10^3}(j,k)$, using the Γ_B (left plots) and Γ_G (right plots) scattering matrices. Formulations 1, 7, 10 (all having the same P_n patterns) in (a) and (b); formulation 2 in (c) and (d); and formulation 6 in (e) and (f).

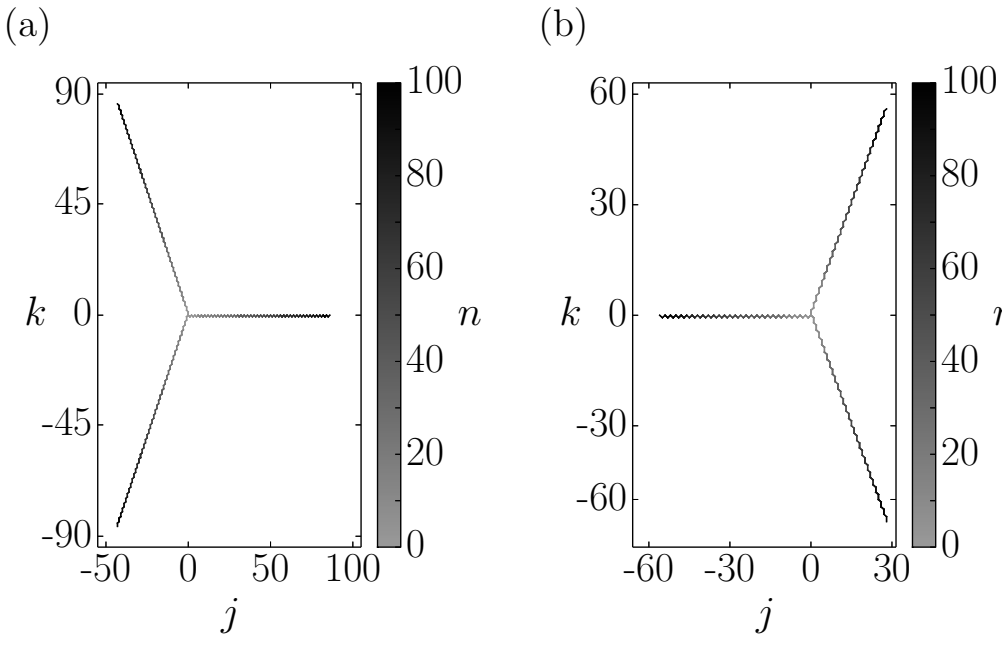

Figure 25: For formulation 2 with (a) Γ_B and (b) Γ_G, the highest values of $P_n(j,k)$ for the number of steps n from 1 to 100. The pattern in (a) is exactly that of the CPs in the Fig. below (a).

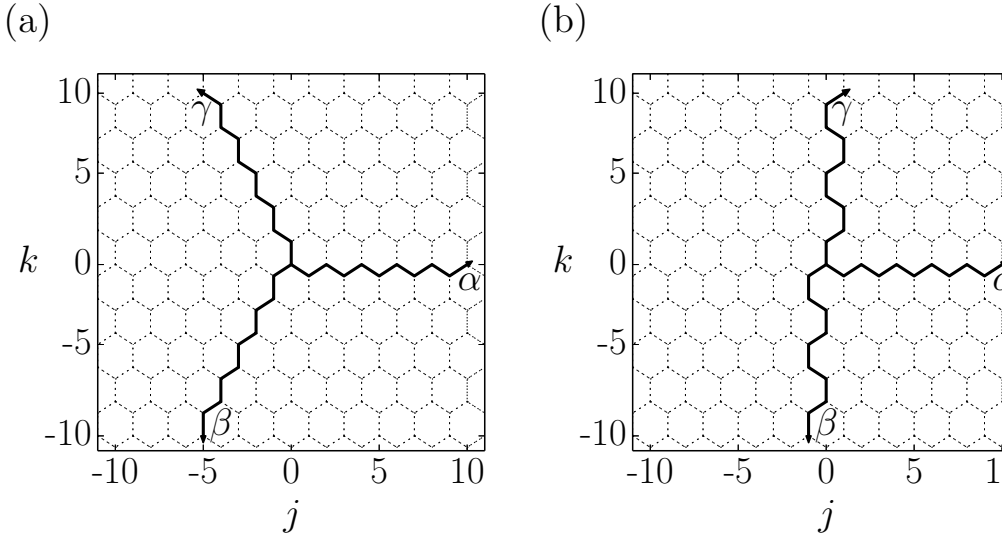

Figure 26: The characteristics paths $\sigma = \alpha, \beta, \gamma$ for the formulations (a) 2 and (b) 6.

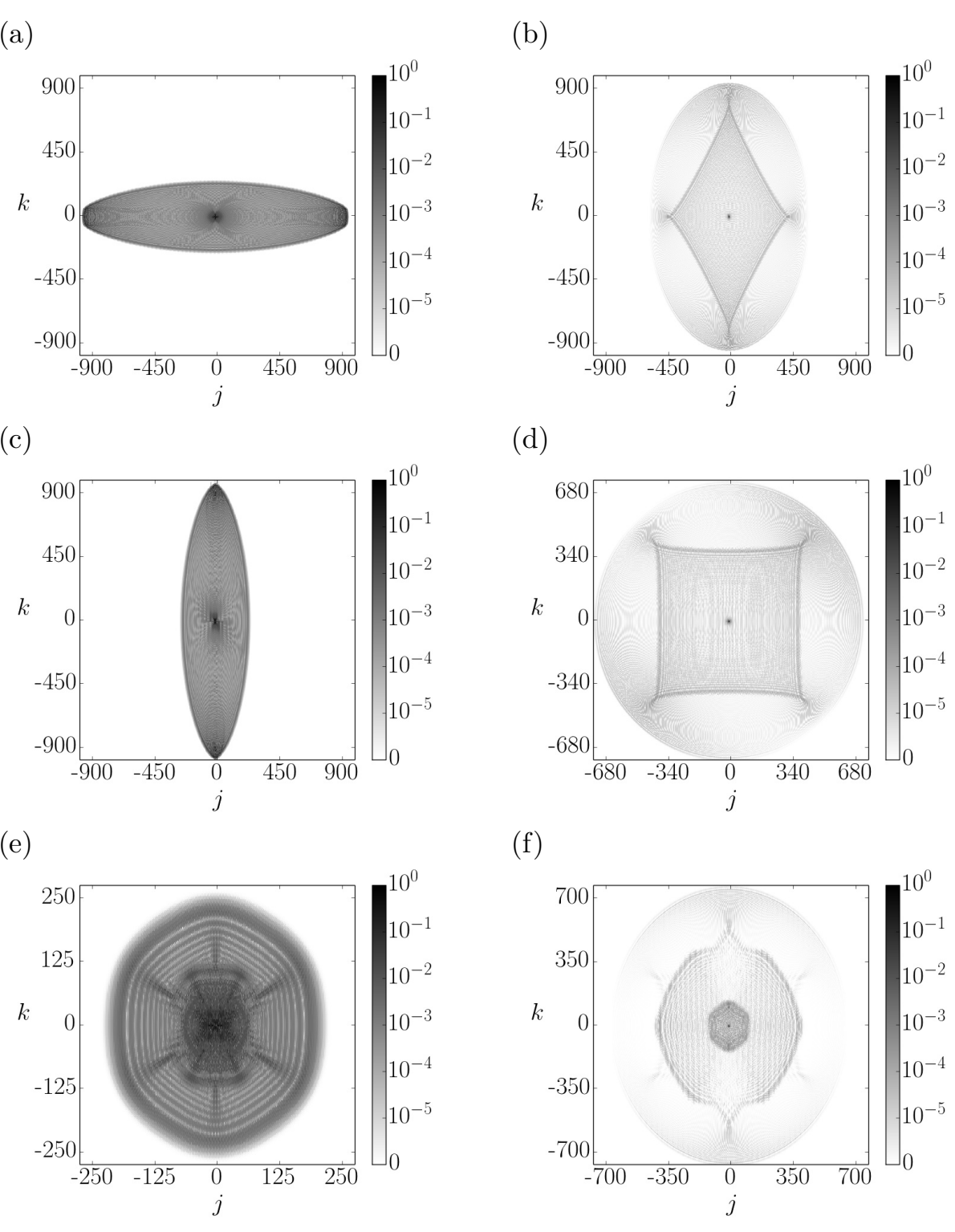

Figure 27: The same as in Fig. 24, but for formulations 3 and 4 (which are Γ-PD for these scattering matrices) with (a) Γ_B and (b) Γ_G, formulation 5 with (c) Γ_B and (d) Γ_G, and formulation 8 with (e) Γ_B and (f) Γ_G.

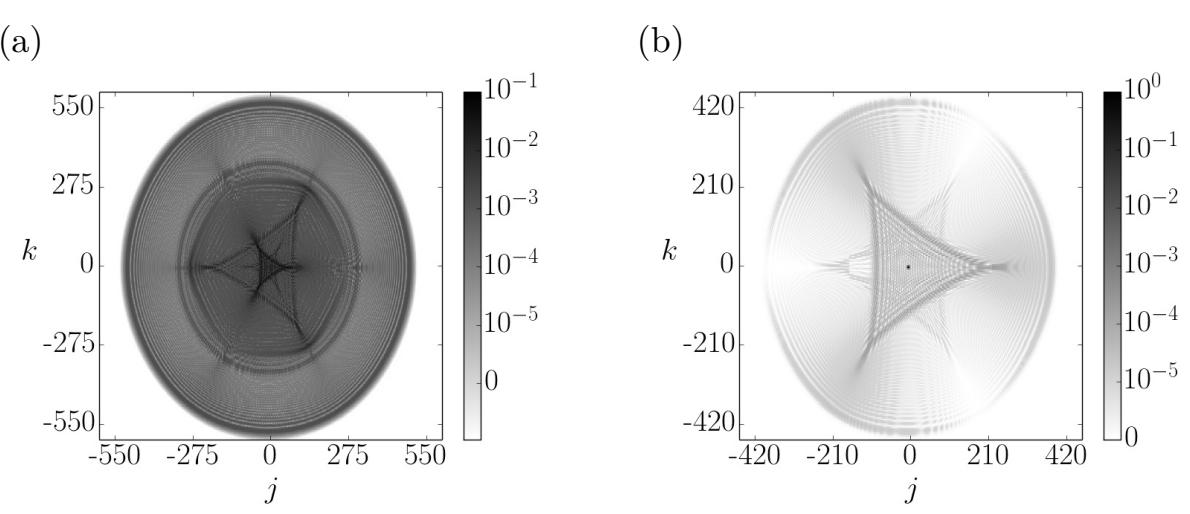

Figure 28: The same as in Fig. 24, but for formulation 9 with (a) Γ_B and (b) Γ_G.

Many thanks Varna!

7 500 B.C.: perhaps a flood in the Black Sea

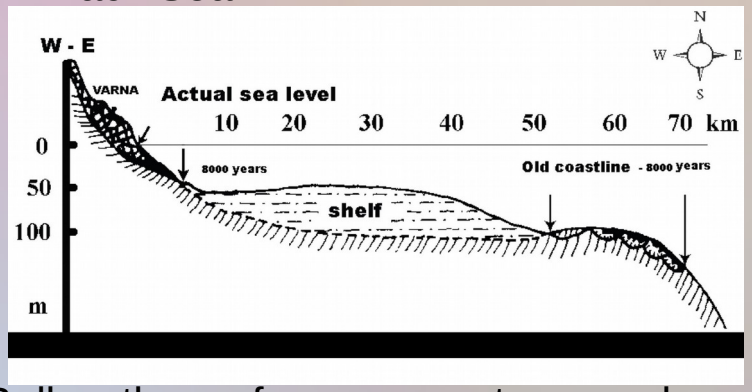

The myth of Jason and the argonauts

Medieval map

Bellow the surface, many stone made villages could be found: perhaps a very advanced civilization of the VI-V millennium BC